Redox-dependent condensation of mycobacterial genome by WhiB4

Manbeena Chawla[1], Mansi Mehta[1#],Pankti Parikh[1#], Saurabh Mishra[1], Prashant Shukla[1,2], Priyanka Baloni[3], Manika Vij[4,5], H N Verma[6], Munia Ganguli[4,5], Nagasuma Chandra[3] and Amit Singh[1*]

[1] Department of Microbiology and Cell Biology, Centre for Infectious Disease Research, Indian Institute of Science, Bangalore 560012, India

[2] Immunology group, International Centre for Genetic Engineering and Biotechnology, New Delhi 110067, India

[3] Department of Biochemistry, Indian Institute of Science, Bangalore 560012, India

[4] Department of Structural Biology, CSIR-Institute of Genomics and Integrative Biology, South Campus, Mathura Road, New Delhi 110020, India

[5] Academy of Scientific and Innovative Research (AcSIR), Anusandhan Bhawan, 2 Rafi Marg, New Delhi 110001, India

[6] Jaipur National University, Jagatpura, Jaipur 302017, India

# These authors contributed equally to this work.

*** Correspondence:**

Amit Singh,
Assistant Professor,
Department of Microbiology and Cell Biology (MCBL)
Centre for Infectious Disease and Research (CIDR)
Indian Institute of Science (IISc)
Bangalore, India-560012
asingh@mcbl.iisc.ernet.in
Ph: 080-22932604

Abstract

Conventionally, oxidative stress response in bacteria is mediated through coordination between the regulators of oxidant-remediation systems (*e.g.* OxyR, SoxR) and nucleoid condensation (*e.g.* Dps, Fis). However, *Mycobacterium tuberculosis* (*Mtb*) lacks these mechanisms. Therefore, how *Mtb* organizes genome architecture and regulates gene expression to counterbalance oxidative imbalance during infection is not known. Using systems biology and imaging techniques, we report that an intracellular redox-sensor, WhiB4, dynamically regulates genome condensation and multiple oxidative stress response networks in *Mtb*. Notably, a low degree of oxidative stress induced marginal genome condensation, while heightened oxidative stress triggered mycobacterial death through nucleoid hyper-condensation. Deletion of WhiB4 alleviated, whereas over-expression aggravated the negative impact of DNA condensation on oxidative stress survival of *Mtb*. Further, our results suggest that WhiB4 mediates both architectural and regulatory roles by controlling auto-expression, homo-interaction, and hetero-interaction with sigma factors, SigE and SigA, in response to changes in intramycobacterial redox potential. Over-expression of WhiB4 in *Mtb* disrupts redox homeostasis, damages genome integrity, and synergizes with host-generated radicals to exert efficient killing inside macrophages and mice. Expression of SigE counteracted the deleterious influence of WhiB4 over-expression on nucleoid condensation and survival, indicating that WhiB4-SigE constitutes a system that calibrates oxidative stress response in *Mtb*. We infer that WhiB4 is a novel redox-dependent architectural protein that structurally couples response to oxidative stress with changes in genome organization and transcription in *Mtb*. This previously unidentified dependence of *Mtb* on WhiB4 and

nucleoid condensation to modulate oxidative stress response expands our understanding of bacterial pathogenicity.

Author Summary

In pathogenic mycobacteria, understanding of the concerted rearrangements of gene activities during various stages of infection is a fundamental problem. To persist, *Mtb* needs to adapt in response to an array of successive environmental challenges encountered during infection. Most of the hostile conditions within host, including acidic and oxidative stress, are known to induce changes in DNA topology in other bacterial systems. Variations in nucleoid condensation in response to changing environmental conditions may serve as a signal triggering the virulence program during the infection process. We deciphered a redox-based mechanistic device, WhiB4, coordinating the chromosomal structure with selective expression of the adaptive traits in response to oxidative stress. Using a holistic approach exploring the inherent relationships between the physicochemical properties of the DNA, cytoplasmic redox potential, and regulation of virulence factors network mediating adaptive potential in *Mtb*, we uncovered a fundamental basis of oxidative stress tolerance and mycobacterial persistence during infection.

Introduction

Mycobacterium tuberculosis (*Mtb*) is the causative agent of Tuberculosis (TB), which is one of the major global health problems faced by the humans. Upon aerosol infection, *Mtb* is phagocytosed by alveolar macrophages, where it is exposed to different hostile conditions like reactive oxygen and nitrogen species (ROS and RNS), nutrient starvation, acidic pH and antimicrobial peptides [1, 2]. Among host-generated stresses, contribution of redox stress in controlling proliferation of *Mtb* has been studied in detail. For example, mice deficient in ROS and RNS generating enzymes, NADPH oxidase (NOX-2) and inducible nitric oxide synthase (iNOS), respectively, showed greater susceptibility to *Mtb* infection [3-6]. Clinical relevance of oxidative stress comes from studies demonstrating increased susceptibility of children with defective NOX-2 to infections caused by *Mtb* and BCG [7]. However, despite an oxidative environment faced by *Mtb* inside macrophages, it has a remarkable capacity to induce adaptive mechanisms to resist redox stress [8]. To counter redox stress, *Mtb* encodes proteins such as AhpC/D (alkyl hydroperoxidase), KatG (catalase), SodA and SodC (superoxide dismutases), TrxA, TrxB and TrxC (thioredoxins), glucose-6-phosphate dehydrogenase, MsrA/B (methionine-sulfoxide reductase) and membrane-associated oxidoreductase complex (MRC) [9, 10]. Additionally, cytoplasmic antioxidants like mycothiol (MSH) and ergothioneine (ERG) further dissipate redox stress during infection [11, 12].

Apart from these response mechanisms, bacterial nucleoid also undergoes dynamic changes in its architecture in response to stresses such as ROS, RNS, osmolarity, and pH [13]. Nucleoid associated proteins (NAPs) including Dps (DNA-

binding protein from starved cells) and Fis (Factor for inversion stimulation) in *E. coli*, MrgA (Metallo regulated genes A) in *Staphylococcus aureus*, DR0199 (homolog of EbfC) in *Deinococcus radiodurans*, HU (homolog of Hup protein) in *Helicobacter pylori* and Lsr2 in *Mtb* protect bacterial cells from Fenton-mediated oxidative damage by physically shielding and compacting genomic DNA [14-18]. Moreover, while regulated condensation of nucleoid protects cells against oxidative stress, long-lasting condensation has been shown to stimulate oxidative-stress mediated death by interfering with normal cellular processes such as replication and transcription [19]. Despite the recognized importance of NAPs in modulating oxidative stress response, identity of protein(s) that monitors changes in the cytoplasmic redox potential of bacteria to directly sculpt genome architecture in response to oxidative stress remains elusive in prokaryotes. Previously, we have shown that *Mtb* WhiB4 is required to regulate survival in response to oxidative stress *in vitro* [20]. However, the fundamental mechanism of how WhiB4 coordinates oxidative stress response in *Mtb* remained uncharacterized. Although several studies have broadly demonstrated the role of WhiB proteins (WhiB1 to WhiB7) in regulating gene expression and controlling a plethora of functions including antibiotic resistance, oxidative/nitrosative/acidic stress response, immune-response, cell division, and secretion [9, 21, 22], the mechanistic basis of how WhiB proteins act inside *Mtb* remains poorly studied.

In this study, we employed multiple analytical techniques including microarray, graph-theory based network analyses, electrophoretic mobility shift assays (EMSAs), atomic force microscopy (AFM), and confocal microscopy to examine the role of WhiB4 in governing nucleoid condensation and regulating gene expression upon

oxidative stress. Further, using a non-invasive biosensor of mycothiol redox potential (E_{MSH}, Mrx1-roGFP2), we present evidence that WhiB4 regulates E_{MSH} to modulate survival under oxidative stress conditions during infection. Lastly, we provide compelling data to show a functional linkage between intramycobacterial E_{MSH} and genome compaction in *Mtb* and demonstrate how WhiB4–mediated regulation of nucleoid architecture influences survival inside macrophages and in mice. Taken together, we show a novel WhiB4-coordinated redox-regulatory mechanism to control mycobacterial virulence by dynamically manipulating DNA architecture and expression at the genomic level.

Results

Network mining revealed the role of WhiB4 in controlling multiple oxidative stress responsive pathways in *Mtb*

To investigate the fundamental mechanism underlying WhiB4-mediated regulation of *Mtb* survival under oxidative stress, we first generated an unmarked strain of *Mtb* lacking the entire open reading frame (ORF) encoding WhiB4 (S1 Fig).

Next, we performed global transcriptome profiling of wt *Mtb* and *MtbΔwhiB4* in response to a non-toxic concentration of an oxidant, cumene hydroperoxide (0.25 mM CHP for 2 h). Several genes were found to be differentially regulated in wt *Mtb* and *MtbΔwhiB4* in response to CHP [(log values) 2-fold up- and down- regulation, $p \leq 0.05$] (S1 Table), indicating both positive and negative influence of WhiB4 loss on gene expression. Functional classification of these genes indicates differential regulation of genes belonging to diverse pathways such as central metabolism, virulence, gene regulation, and lipid metabolism (S2 Fig).

The *whiB4*-dependent expression of some of the CHP responsive genes was validated by quantitative RT-PCR (qRT-PCR) (S2 Table). Although informative, expression profiling provides very little insight on how and why multiple genes with varied functions cooperatively respond to oxidative stress in *Mtb*. To gain mechanistic insights into such a complex dataset, a systems based approach exploiting both the genome-wide protein interaction network and transcriptomic data is required. We and others have demonstrated the application of integrating global protein interaction map and expression data to reveal dynamic changes in cellular networks associated with drug resistance and latency in *Mtb* at a genomic scale [23, 24]. To do this, we first constructed a curated and most up-to-date global protein-protein interaction network of *Mtb* and carried out network analyses by employing a well-established graph theoretical method (see SI Materials and Methods and S1 Note). The interaction network generated consists of 3651 proteins and 34035 interactions, covering approximately 90.86% of the *Mtb* proteome (S1 Note, S3 Table). Nodes in the network represent individual proteins and the edges represent interactions among them (S1 Note, Table S3). Using this network, specific oxidative stress response networks were derived by integrating the global expression data obtained upon treatment of wt *Mtb* and *MtbΔwhiB4* with CHP (S1 Note, S3 Table). From this, WhiB4-mediated changes in the oxidative stress network are elucidated.

We first examined the topmost activities operational in wt *Mtb* and *MtbΔwhiB4* under oxidative stress using a network mining approach as described earlier [23]. Briefly, highest activity paths captured in an unbiased manner represent major processes taking place in *Mtb* in response to oxidative stress as compared to

unstressed cells. Each path contains a set of nodes, some showing differential expression, connected to each other in the network. In wt *Mtb*, we found that the top-paths form a reasonably well connected network, thus generating a sub-network of the larger protein-protein interactions network (Fig. 1). Several mechanisms known to respond to oxidative stress feature in the top-paths sub-network of CHP treated wt *Mtb*. These include; (a) chaperones involved in repairing oxidatively damaged proteins, [*dnaK*, *hsp*, *dnaJ1*, *dnaJ2*, *grpE*, *clpC, clpB*], (b) genes involved in neutralizing ROS [*ahpC*, *ahpD*, *trxC*, *trxB2*, *trxB1*, *trxA*, *katG*], (c) stress responsive sigma factors [*sigH*, *sigE*, *sigB*], and (d) redox-/iron-sensing transcription factors [*whiB3,whiB1,furA , clgR, and ideR*] (Fig. 1, S3 Table). We observed a number of top-nodes associated with sulphur uptake, Fe-S biogenesis, and cysteine biosynthesis, indicating a major role for sulfur metabolism in tolerating oxidative stress (Fig 1, S3 Table). Interestingly, most of the nodes within functionally diverse modules converge at a common stress responsive protein folding chaperone, DnaK, making it a major hub node, and protein homeostasis a central mechanism coordinating oxidative stress response in *Mtb* (Fig. 1, S3 Table). In other bacterial species, dynamic changes in the nucleoid condensation state directed by several NAPs and assisted by topology regulating enzymes such as DNA gyrases and topoisomerases protects against oxidative stress [16, 25, 26]. Surprisingly, neither NAPs nor topology enzymes (*gyrA, topA*) were found to be the part of topmost active paths in *Mtb* upon CHP treatment conditions used in our study. Microarray analysis showed that *gyrA* and *topA* were down-regulated and expression of NAPs (*espR, lsr2, and hupB*) was unaffected upon oxidative stress in *Mtb* (S1 Table). Together, these findings indicate a larger role for antioxidants pathway and protein repair

machinery in controlling oxidative stress, whereas known mechanisms of genome condensation likely plays a minor role in *Mtb*.

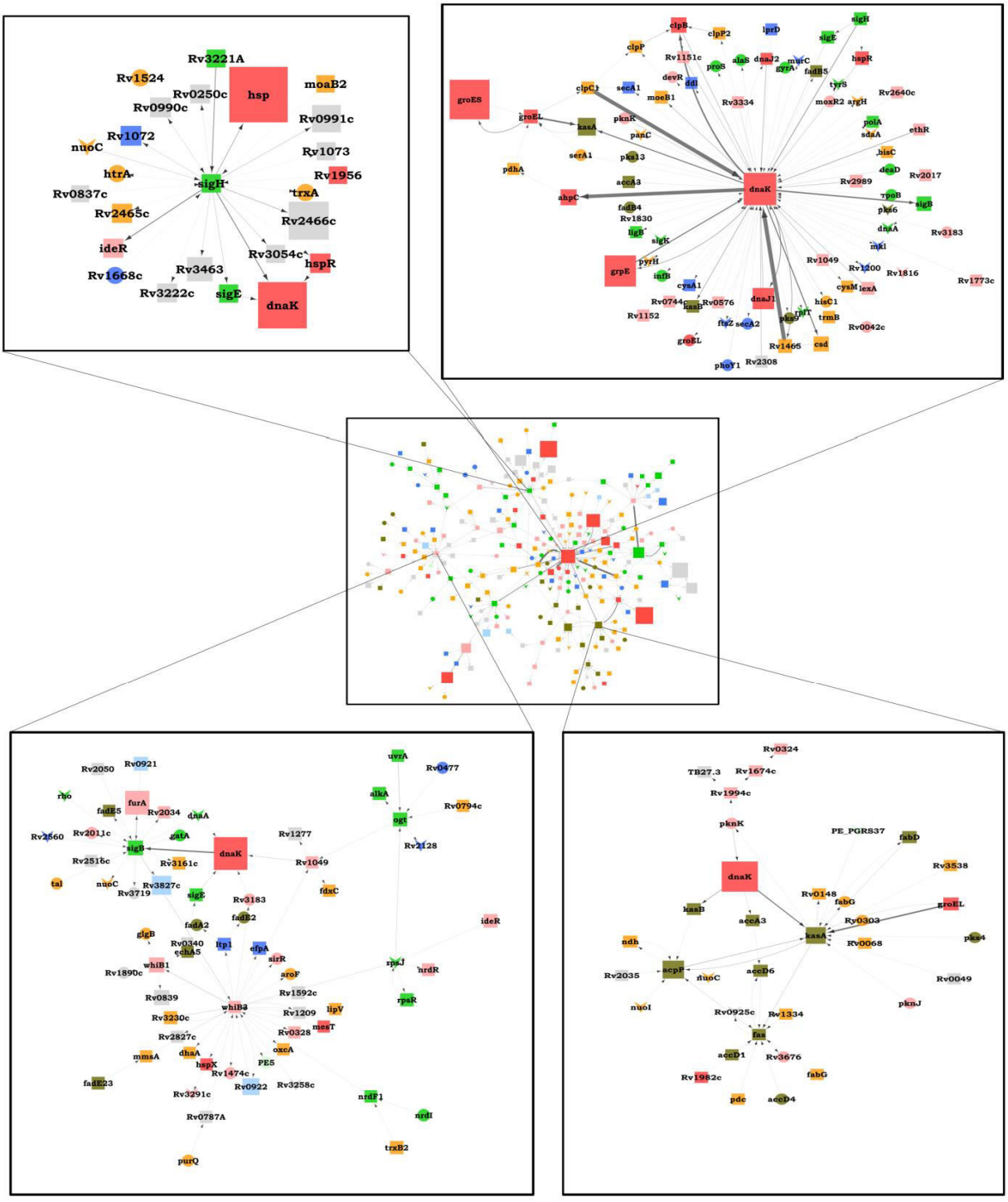

Fig. 1: Oxidative stress network of wt *Mtb*. The expression data of wt *Mtb* treated with CHP vs. untreated wt *Mtb* was superimposed on *Mtb* protein-protein interaction network (See SI note 1). The sub-network obtained depicts the top-most activities in wt *Mtb* upon CHP treatment. The nodes (genes) are denoted by circles (non-differentially regulated genes), squares (up-regulated) and inverted arrow-heads (down-regulated). The size of the node indicates its node weight or higher

signal intensity. The interactions/edges are depicted by grey arrows, the thickness of the arrows being a measure of the strength of the interactions. The nodes are colored according to the TubercuList functional categories – red: virulence, detoxification, and adaptation, blue: cell wall and cell processes, green: information pathways, yellow: intermediary metabolism and respiration, olive green: lipid metabolism, grey: conserved hypotheticals, pink: regulatory proteins, cyan: insertion sequences and phages, and light green: PE/PPE family.

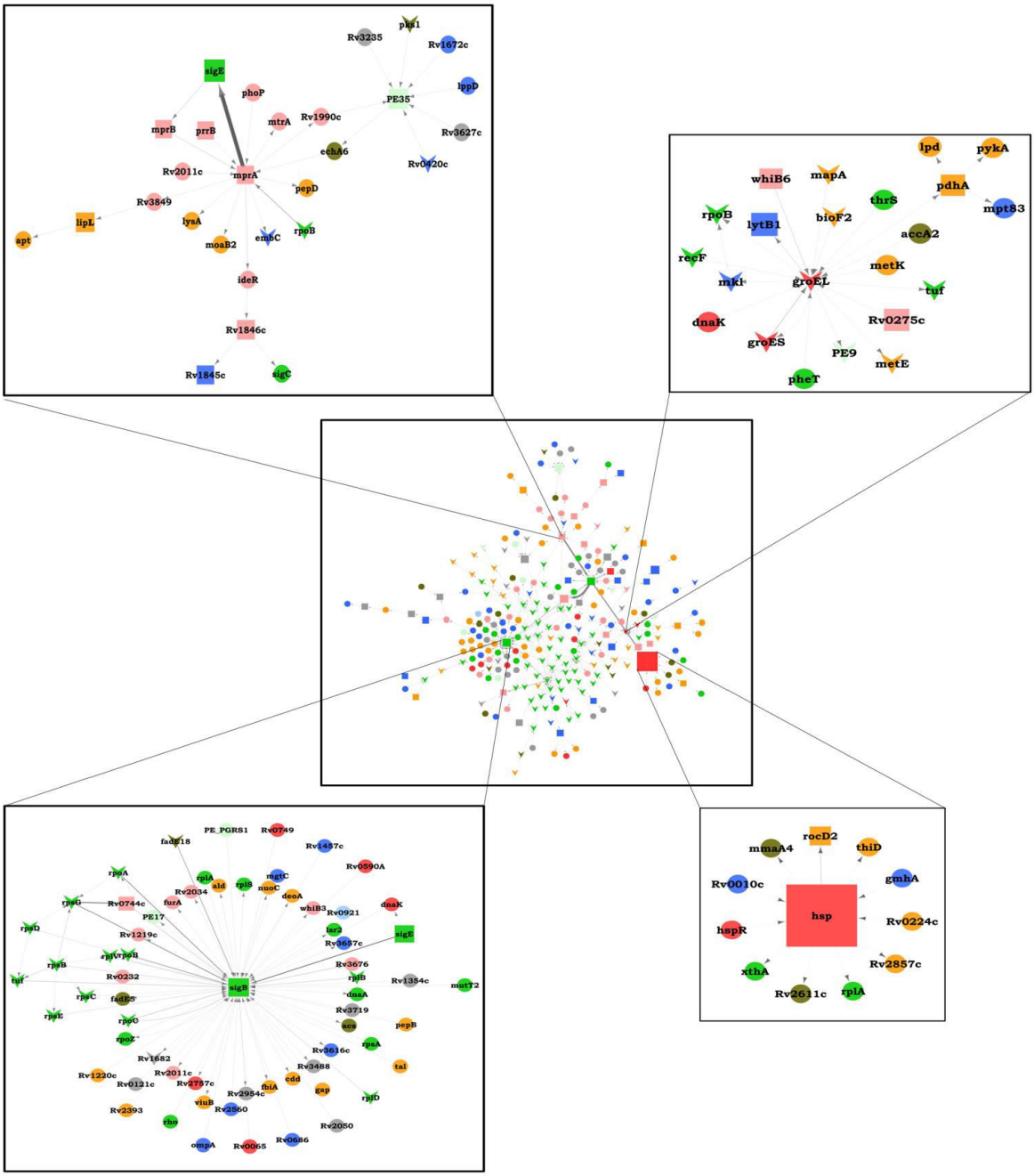

Fig. 2: Oxidative stress network of *MtbΔwhiB4*. The sub-network obtained was generated by overlaying expression data of CHP treated *MtbΔwhiB4* vs. untreated *MtbΔwhiB4* as described in the legend for figure 1. The top-most activities operational in CHP treated *MtbΔwhiB4* were shown. The network description is similar to the legend of figure 1.

Next, we analyzed how CHP influences topological properties of oxidative stress network in *MtbΔwhiB4* in comparison to untreated *MtbΔwhiB4* (Fig. 2). We found that the stress network is restricted to only a select set of hub nodes in CHP treated *MtbΔwhiB4*. The top-most active paths include a sub-network of genes associated with *sigB, sigE,* and *hsp* (Fig. 2).

A strong interaction was observed among the factors involved in mediating oxidative stress and cell wall associated stress in *MtbΔwhiB4* upon CHP treatment. This includes *sigB, sigE, mprA, and sigH* nodes, indicating a functional association between WhiB4 redox regulatory pathway and the network formed by stress responsive sigma factors (Fig. 2). To completely identify the repertoire of interactions specifically influenced in *MtbΔwhiB4* in comparison to wt *Mtb* under oxidative stress, we adopted an approach in which networks common in wt *Mtb* and *MtbΔwhiB4* under normal and stressed conditions were subtracted to identify unique nodes and edges that are significantly activated only in *MtbΔwhiB4* under oxidative stress (see S2 Note, S3 and S4 Tables). Identification of top-most activities revealed hallmarks of diverse oxidative stress remediation mechanisms specifically activated in *MtbΔwhiB4* (Fig. 3). For example, a major network of central carbon metabolic (CCM) enzymes, which also participate in anti-oxidative and anti-nitrosative activities, was highly induced in *MtbΔwhiB4.* This includes *pdhABC, lpdA, dlaT,* and *ahpCD*, all of which serve as functional subunits of CCM enzymes - pyruvate dehydrogenase (PDH), α-ketoglutarate (α-KG) dehydrogenase, and branched chain keto-acid dehydrogenase (BKADH) (Fig. 3) [27-30]. Likewise, DNA repair machineries including SOS response (*lexA and recA*), nucleotide excision repair

(*uvrD1*), alkylated DNA repair (*alkB, Rv3916c*) and recombinational repair (*ruvA – ruvC*) were activated in *MtbΔwhiB4* (Fig. 3).

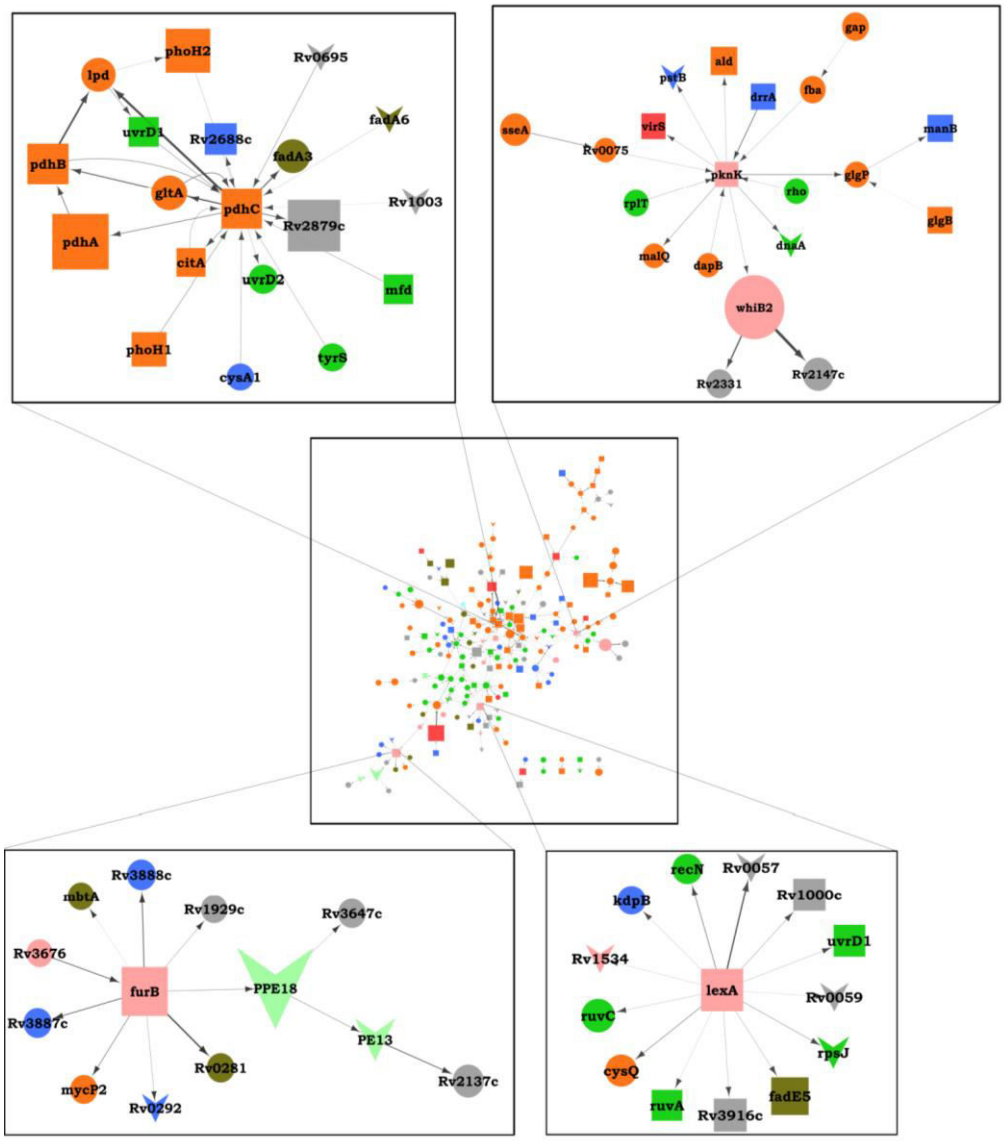

Fig. 3 Network subtraction revealed the identity of WhiB4-specific responses under oxidative stress. The WhiB4-specific sub-network was constructed by extracting edges and nodes unique to *MtbΔwhiB4* as compared to wt *Mtb* under oxidative stress (See Note 2 SI). The network depiction is similar to the legend for Figure 1.

Not surprisingly, deletion of CCM (*dlaT, lpdA*) and DNA repair genes (UvrD1) in *Mtb* resulted in heightened susceptibility to ROS, RNS, and loss of virulence *in vivo* [29, 31]. Lastly, several transcription factor modules involved in redox

homeostasis (*whiB2 and furB*) and virulence regulation (*pknK, virS, and Rv3676*) form a network of interconnected nodes in *MtbΔwhiB4* (Fig. 3). Altogether, higher antioxidants capacity, activated DNA repair genes, and regulation of stress responsive transcription factors/sigma factors provide a likely explanation for our earlier study showing higher oxidative stress survival and hypervirulent phenotypes of *MtbΔwhiB4* [20].

Mtb WhiB4 exhibits non-specific DNA binding

Having shown that WhiB4 disruption is associated with large changes in the expression of oxidative stress responsive genes, we next sought to examine the underlying mechanism of WhiB4-mediated gene regulation. The role of *Mtb* WhiB proteins in regulating transcription is mostly attributed to their interaction with the principal sigma factor, SigA [32, 33]. However, DNA binding properties of WhiB proteins are distinct from classical DNA binding transcriptional regulators. For example, a clear DNA binding domain (*e.g.,* HTH motif) is absent in WhiB proteins, rather a series of C-terminus basic residues are likely responsible for mediating their interaction with non-specific DNA sequences [34-36]. Agreeing to this, several DNA binding studies *in vitro*, and genome-wide analysis *in vivo*, failed to identify any DNA binding consensus sequences for WhiB proteins in actinomycetes, including mycobacteria [35-38]. Lastly, C-terminus of WhiB7 contains a characteristic AT-hook motif, which is naturally associated with non-specific DNA binding proteins involved in coordinating genome architecture such as high-mobility group (HMG) non-histone nuclear proteins [36, 39]. Altogether, till date, no WhiB like protein (Wbl) has been conclusively shown to interact with specific DNA sequences *in vivo*, indicating a

hitherto unknown role for non-specific DNA binding of WhiB proteins in their biological function.

We have previously shown that WhiB4 possess a 4Fe-4S cluster (holo-WhiB4), which can be rapidly degraded by atmospheric oxygen to generate disulfide-linked oligomers of clusterless WhiB4 (oxidized apo-WhiB4). Holo-WhiB4 lacks DNA binding capacity, whereas disulfide-linked oligomers of apo-WhiB4 binds DNA in a sequence independent manner with a preference for GC-rich sequences [20]. WhiB1, WhiB2 and WhiB3 were also shown to interact strongly with DNA in their apo-forms [36, 40, 41]. Using microarray data, we selected a new set of genes differentially regulated by CHP in a WhiB4-dependent manner and repeated DNA binding assays. Oxidized apo-WhiB4 consistently binds to the DNA fragments (S3A Fig). However, binding seems to be non-specific as WhiB4 binds to both the intergenic and coding regions of oxidative stress responsive genes with comparable affinities (K_d = 1.5-2.5 μM; S3A Fig). As found earlier, DNA binding was increased with an increase in the GC content of DNA fragments (S3B Fig). *In vivo* thiol-trapping experiment revealed that CHP stress further increased the ratio of disulfide-linked oligomeric forms of apo-WhiB4 vs. monomeric-reduced WhiB4 inside *Mtb* (S4 Fig), indicating that oxidized apo-WhiB4 form is biologically relevant under oxidative stress conditions. Similar to CHP stress conditions, ectopic expression of WhiB4 was previously shown to increase the abundance of oxidized apo-WhiB4 form inside mycobacteria under normal growing conditions [20]. To understand the relevance of oxidized apo-WhiB4 DNA binding *in vivo,* we over-expressed a FLAG-tagged version of WhiB4 in *MtbΔwhiB4* (WhiB4-OE) and determined the occupancy of WhiB4 by chromatin immunoprecipitation combined with quantitative PCR assay (ChIP-qPCR)

on a set of promoter regions of genes showing opposite expression in *MtbΔwhiB*4 as compared to wt *Mtb* in microarrays.

Table 1: ChIP-qPCR for occupancy enrichment of WhiB4.

Genes	**Microarray** Fold change (CHP treated *wt Mtb*/ wt *Mtb*)	**Microarray** Fold change (CHP treated *MtbΔwhiB4*/ *MtbΔwhiB4*)	**Microarray** Fold change (CHP treated *MtbΔwhiB4*/ CHP treated wt *Mtb*)	**qRT PCR** Fold change (*whiB4-OE*/ *MtbΔwhiB4*)	**qRT PCR** Fold change (CHP treated *whiB4-OE*/ CHP treated *MtbΔwhiB4*)	**ChIP-qPCR** Fold enrichment values	**GC %**
Rv0005 (*gyrB*)	1.604	1.29	0.72	-3.90 ±0.22	-4.50 ±0.24	17.26	68
Rv0251c (*hsp*)	26.8	37.2	1.316	-6.69 ±0.60	-1.37 ±0.24	36	69
Rv1182* (*papA3*)	0.97	0.72	0.58	-1.23±0.31	-1.1±0.08	0.98	61
Rv1470* (*trxA*)	0.83	2	0.83	-1.15±0.03	-1.04±0.1	1.31	60
Rv2428 (*ahpC*)	4.3	1.58	2.26	-3.85 ±0.49	-10.67 ±1.52	4.1	65
Rv2429 (*ahpD*)	5.08	1.66	2.047	-6.66 ±0.46	-9.24 ±0.29	3.35	65
Rv2710 (*sigB*)	4.16	6.2	1.50	-1.31 ±0.16	-1.52 ±0.28	2.82	64
Rv3223c (*sigH*)	3.46	1.22	1.61	-2.51 ±0.24	-1.67 ±0.22	2.39	66
Rv3283* (*sseA*)	0.91	1.38	0.89	-1.1±0.23	-0.69±0.13	1.61	60
Rv3914 (*trxC*)	4.8	1.2	0.77	-3.90 ±0.43	-1.61 ±0.34	11.56	68

* Genes not affected by WhiB4 were taken as negative controls. *MtbΔwhiB4* served as a negative control in ChIP-qPCR assays. Fold enrichment values for each target was calculated as described in materials and methods

The *MtbΔwhiB4* strain was used as a negative control. Using various oligonucleotide combinations, an ~ 400 bp upstream of coding regions was scanned by ChIP-qPCR to detect WhiB4 binding. Data for the regions showing a significant WhiB4 enrichment (≥2-fold; *P* value of $<10^{-3}$) are shown. WhiB4 functions as an autorepressor by binding to its own promoter [20]. A significant enrichment of WhiB4 was observed around its promoter region, thus validating our approach (Table 1). Variable but significant enrichment was detected with most of the WhiB4-specific genes identified in microarray (Table 1). Importantly, degree of WhiB4 enrichment is reasonably consistent with the expression data. For example, WhiB4 occupancy was enriched on the promoters of genes showing a significant deregulation in *MtbΔwhiB4* and WhiB4-OE (*e.g., gyrB, hsp, trxC*, *ahpCD*, and *whiB4*). Similarly, promoters of marginally affected genes (*e.g., sigB and sigH*) displayed much weaker occupancy, while WhiB4 binding was absent from promoters of unaffected genes (e.g., *papA3* and *sseA)*. In case of *ahpC-ahpD* operon, WhiB4 enrichment was observed both in the promoter region (*i.e.* upstream of *ahpC*) and within the *ahpC* coding sequences (*i.e.* upstream of *ahpD*) (Table 1). Also, in agreement with our *in vitro* data, occupancy enrichment seems to correlate with the GC content of promoter fragments (Table 1). Supporting these observations, microarray data show that the expression of GC-rich PE-PPE gene family was highly deregulated in *MtbΔwhiB4* (22%) as compared to wt *Mtb* (8%) upon CHP treatment (Fig. S2), and ~ 60% of genes significantly affected by WhiB4 loss contain promoter regions (~ 200 bp upstream of ATG) which are highly GC-rich (>70%) as compared to the genome

average (65%). Future experimentations involving ChIP-Seq analysis under defined oxido-reductive conditions will reveal genome-wide consensus binding motif, if any, for WhiB4. Notwithstanding, WhiB4-DNA interactions seem to be non-specific, but the protein has a preference for binding GC-rich sequences. In addition, WhiB4 has a low molecular weight (13.1 kDa) and a highly basic pI (10.28). All of these features are akin to various dual-purpose nucleoid-associated proteins (NAPs: HNS, HU, IHF and Lrp), which simultaneously mediate both nucleoid architecture and gene regulation. However, the redox-dependent DNA binding is exclusive to WhiB4.

Mtb WhiB4 condenses DNA *in vitro* and *in vivo*

To better grasp the fine molecular details of WhiB4 DNA binding, we systematically investigated if WhiB4 has a NAP like activity. Similar to other bacterial NAPs [13, 15], the oxidized apo-WhiB4 formed a high molecular weight complex with a range of DNA substrates (*e.g.,* supercoiled DNA, linearized DNA, and 1kb λ DNA ladder) and inhibited transcription from a standard T7-promoter of pGEM plasmid *in vitro* (Fig. 4). Inclusion of thiol-reductant, dithiothreitol (DTT), or replacement of any cysteine residues with alanine in WhiB4 reversed DNA binding and transcriptional inhibitory activities of oxidized apo-WhiB4 (Fig. 4). We analyzed the expression of 20 WhiB4-specific genes in *WhiB4-OE* strain. Out of these ~ 85% of genes upregulated in *MtbΔwhiB4* displayed a significant down-regulation upon WhiB4 over-expression (S2 Table), indicating that like HNS and Lsr2 [13, 15], WhiB4 has a negative effect on gene expression. Genes showing a comparable expression in wt *Mtb* and *MtbΔwhiB4* remained unaltered upon WhiB4 expression, indicating that WhiB4 has a specific effect on gene regulation.

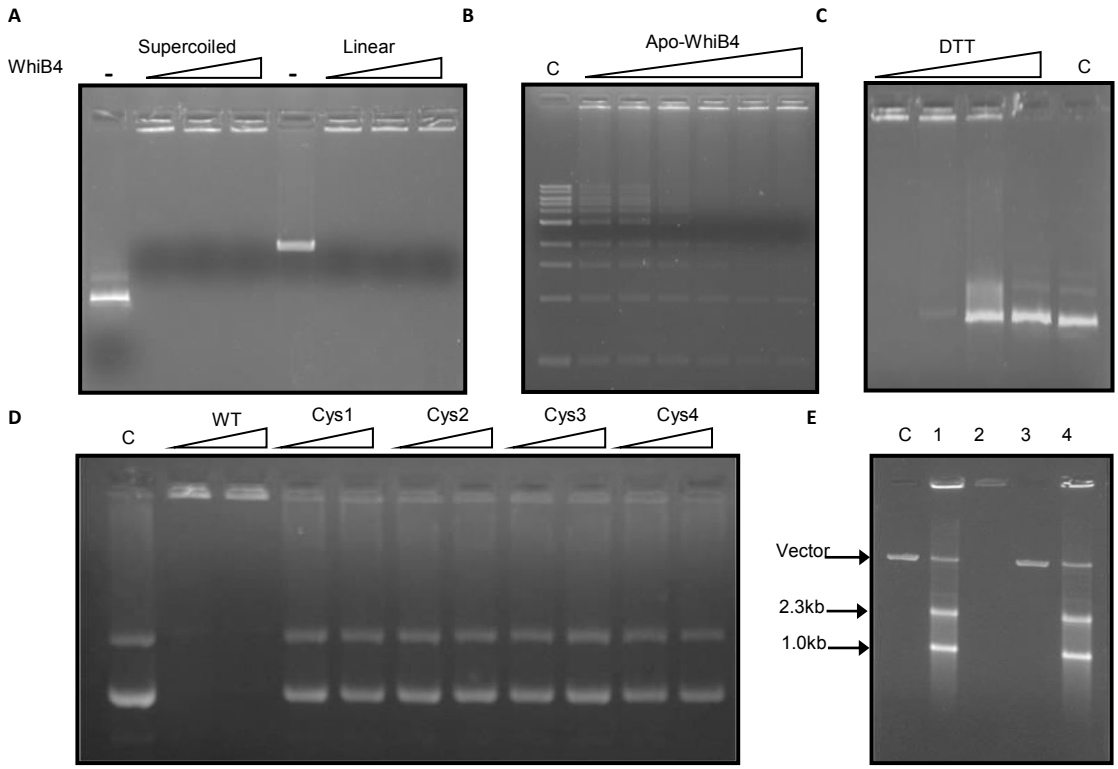

Fig. 4: *Mtb* WhiB4 exhibits non-specific DNA binding activities. (A) 150 ng of either linear or supercoiled plasmid DNA was incubated with oxidized apo-WhiB4 (250 ng [lanes 2, 6]; 300 ng [lanes 3, 7]; 350 ng [4, 8]). Lanes 1 and 5 represent DNA alone control. **(B)** Binding of apo-WhiB4 (100, 150, 200, 250, 300 and 350 ng) with 1kb λ-DNA ladder (150 ng). **Cysteine residues regulate DNA binding of WhiB4**. **(C)** DTT-treatment abolished DNA binding of WhiB4. Oxidized apo-WhiB4 (350 ng) was treated with DTT (0, 200, 400, 800 mM) followed by binding to the supercoiled plasmid DNA. C: represents DNA alone control. **(D)** Purified wt apo-WhiB4 and Cys mutants were treated with thiol oxidant, diamide, and gel-shift assay was performed as described earlier. **(E) WhiB4 represses transcription**. *In vitro* transcribed pGEM plasmid in the absence of apo-WhiB4 (lane 1), oxidized apo-WhiB4 in complex with pGEM (lane 2), *in vitro* transcription of pGEM in the presence of oxidized (Lane 3) or reduced (Lane 4) apo-WhiB4. The reactions in lane 3 and 4 were treated with 6% SDS and 4 mg/ml protease K to remove WhiB4 from the mixture before separation. The samples were analyzed on 1% agarose gel. C: pGEM plasmid DNA alone.

Since NAPs can contribute to both gene regulation and nucleoid structure [13], we propose that WhiB4 can perform both these roles simultaneously in response to oxidative stress in *Mtb*. Therefore, we analyzed DNA compacting ability of oxidized apo-WhiB4 using Atomic Force Microscopy (AFM) *in vitro*. AFM of oxidized apo-WhiB4-DNA complexes revealed condensation of both supercoiled and

relaxed plasmid DNA molecules (Fig. 5C and 5I) where bare apo-WhiB4, relaxed and supercoiled plasmid DNA were taken as experimental controls (Fig. 5A, 5B, 5H).

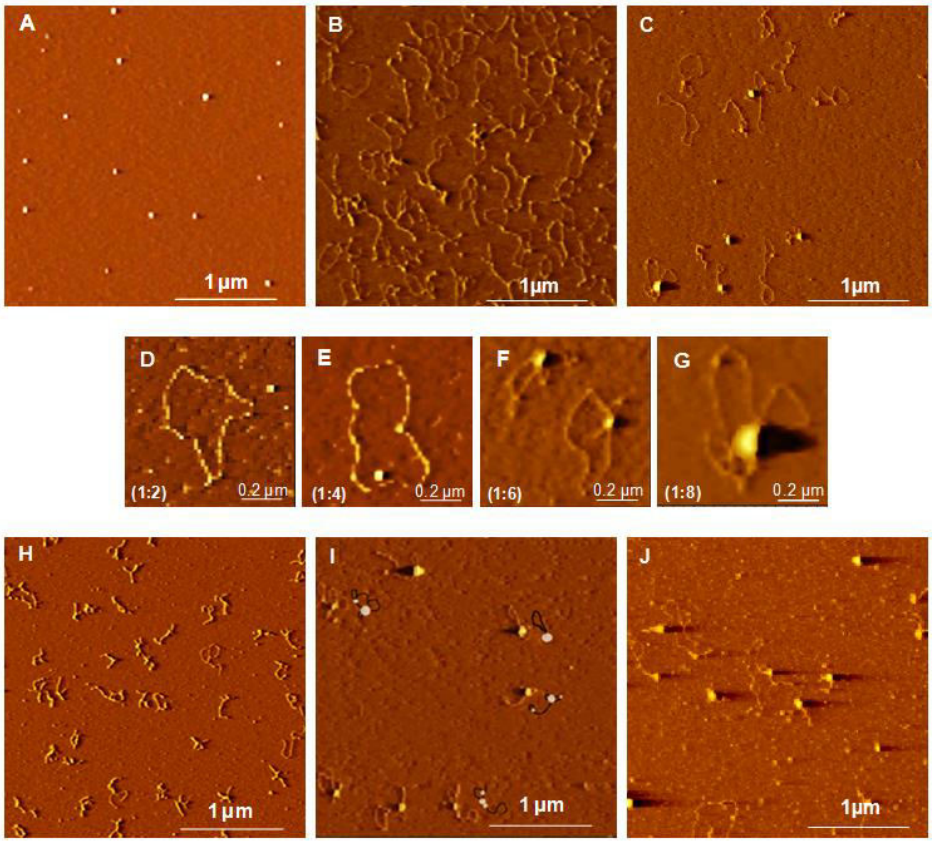

Fig. 5: AFM analysis of WhiB4-mediated DNA condensation. **(A)** Oxidized apo-WhiB4, **(B)** Relaxed plasmid DNA, **(C)** Oxidized apo-WhiB4 incubated with relaxed plasmid. Gradual increase in DNA condensation was observed with increase in DNA:oxidized apo-WhiB4 ratios, **(D)** 1:2, **(E)** 1:4, **(F)** 1:6, and **(G)** 1:8. **(H)** Supercoiled plasmid DNA and **(I)** in complex with oxidized apo-WhiB4. **(J)** The Cys3 mutant of apo-WhiB4 (Cys3-WhiB4) was oxidized by diamide and DNA condensation was monitored by incubation with the relaxed plasmid. The scale of images is 3 µm x 3 µm in panels A, B, C, H, I and J, while D, E, F, G are of 0.8 µm x 0.8 µm.

Increasing the concentration of apo-WhiB4 resulted in the formation of multiple loops within a single plasmid DNA molecule, most likely mediated by the DNA bridging activity of WhiB4 (Fig. 5D, 5E, 5F, and 5G). Importantly, AFM did not reveal DNA condensation in case of a cysteine mutant variant (Cys3-WhiB4) (Fig. 5J),

indicating redox-dependent condensation of plasmid DNA by WhiB4. DNA condensing activity associated with NAPs also confers protection to DNA against DNase I cleavage and iron-dependent hydroxyl radical formation [42]. Oxidized apo-WhiB4 was found to protect DNA from both DNase I and hydroxyl radicals (S5 Fig).

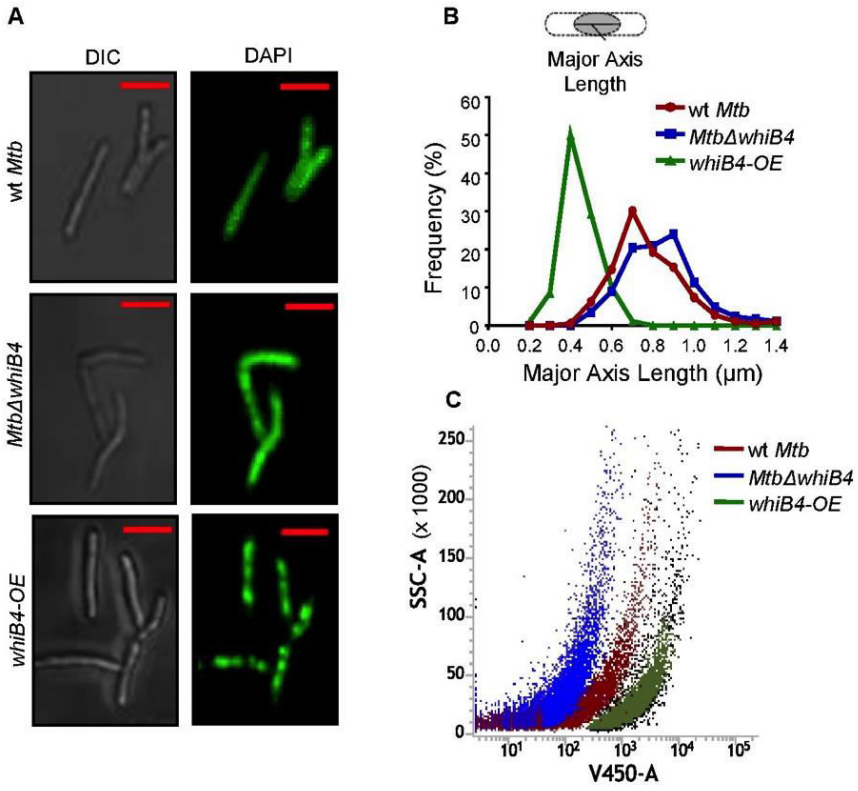

Fig. 6: **WhiB4-mediated nucleoid compaction in *Mtb***. **(A)** Nucleoid of wt *Mtb*, *MtbΔWhiB4* and *whiB4-OE* strains were stained with DAPI (pseudo colored green) and visualized under confocal microscopy (63X). The scale of images is 3μm. **(B)** Histogram showing distribution of the major axis length of the nucleoids in the *Mtb* strains (n= 200 nucleoids/strain). The histogram was generated by plotting the percentage of nucleoids per 0.1 μm size intervals with respect to the major axis length of each nucleoid. **(C)** Flow cytometric analysis of the cell size versus DAPI fluorescence of *Mtb* strains. Increase in fluorescence intensity due to intermediate, lower and higher degree of nucleoid condensation in case of wt *Mtb*, *MtbΔWhiB4* and *whiB4-OE*, respectively, was shown. Experiment was repeated at least twice in triplicate and a representative image is shown.

The biological relevance of DNA condensing activity is generally investigated by examining the nucleoid morphology of cells either over-expressing or lacking the NAPs [43]. To do this, we stained the nucleoids of *wt Mtb*, *MtbΔwhiB4*, and *whiB4-OE* strains using 4',6-diamidino-2-phenylindole (DAPI) and nucleoid compaction was determined by measuring the length of the major axis of more than 200 nucleoids/ strain (Fig. 6). The histogram generated confirmed that *MtbΔwhiB4* and *whiB4-OE* strains differed significantly from wt *Mtb* (p value = 0.0002 and <0.0001 respectively, Mann-Whitney U-test). Average nucleoid lengths were 0.7 μm, 0.9 μm, and 0.4 μm for wt *Mtb*, *MtbΔwhiB4*, and *whiB4-OE* strains, respectively (Fig. 6A and 6B). Flow cytometric analysis of cell size versus DAPI fluorescence intensity confirmed highest compaction in case of *whiB4-OE* strain and lowest in *MtbΔwhiB4* (Fig. 6C). Interestingly, while wt *Mtb* and *whiB4-OE* strains displayed distribution of majority of the nucleoids in a single population, three peaks were clearly apparent at 0.7 μm, 0.8 μm, and 0.9 μm in *MtbΔwhiB4* (Fig. 6B). These results indicate heterogeneity in the condensation state of *MtbΔwhiB4* genome with an overall shift towards a moderately relaxed architecture. Importantly, the effect of WhiB4 over-expression on condensation was not restricted to *Mtb*, as a comparable degree of genome compaction was induced by WhiB4 in *M. smegmatis* (*Msm*) (S6 Fig). In contrast, over-expression of WhiB4 did not condense the genome of *E. coli* (S6 Fig) consistent with the preference of WhiB4 to bind GC-rich sequences. Alternatively, *E.coli* might lacks *Mtb*-specific accessary factors cooperating with WhiB4 to condense nucleoids.

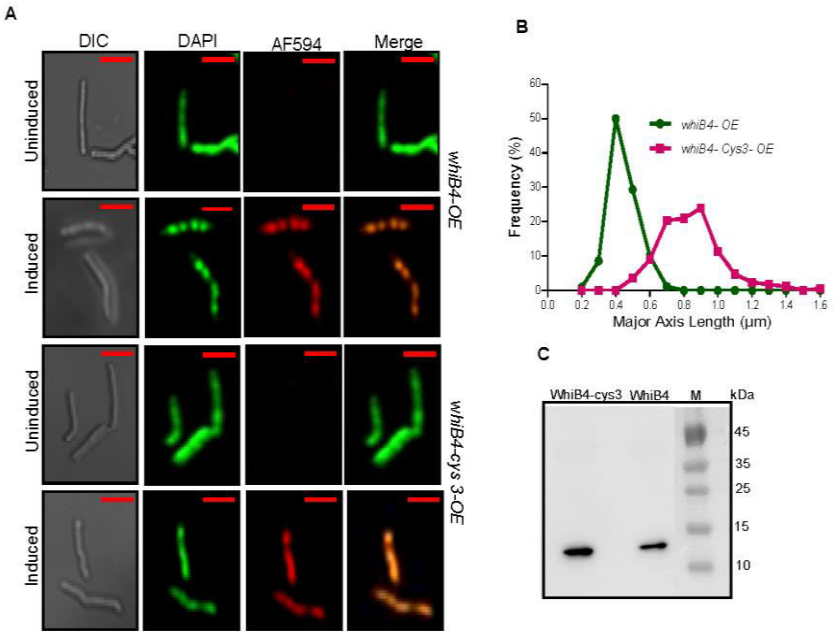

Fig. 7: **Cysteine residues of WhiB4 are important for its DNA condensation activity**. **(A)** Confocal microscopic images (63X) of *MtbΔwhiB4* strain over-expressing WhiB4- and WhiB4-cys3 FLAG tagged proteins. Nucleoids were stained with DAPI (pseudo colored green), wt WhiB4-FLAG and WhiB4-cys3-FLAG mutant were stained with AF594 secondary antibody (red) against anti-FLAG primary antibody, and co-localization was indicated by yellow in the merge panel. The uninduced (UI) control lacks immuno-fluorescence due to absence of WhiB4 expression. The scale of images is 3 µm. **(B)** Histogram showing distribution of the major axis length of the nucleoids in these strains (n=200). The histogram was generated by plotting the percentage of nucleoids per 0.1 µm size intervals with respect to the major axis length of each nucleoid. **(C)** 30 µg of cell free extract from either *whiB4-OE* or *whiB4-cys3-OE* strains were analyzed for the WhiB4 expression by immuno-blotting using antibody against FLAG tag.

Our intracellular localization studies revealed that WhiB4 is exclusively associated with the DAPI-stained clumped nucleoids in the *whiB4-OE* strain (Fig. 7A). In contrast, over-expression of cysteine mutant of WhiB4 (*whiB4-cys3-OE*) did not induce DNA condensation (average nucleoid length = 0.825 µm, $p < 0.0001$ as compared to *whiB4-OE*, Mann-Whitney U-test) and remained associated with the entire length of a cell (Fig. 7A and 7B). Expression of WhiB4 was comparable in both *whiB4-OE* and *whiB4-cys3-OE* strains indicating that the loss of DNA condensation in the *whiB4-cys3-OE* is due to disruption of thiol-disulfide redox switch rather than

altered protein levels (Fig. 7C). Altogether, these results indicate a well-organized redox-dependent compacting mechanism mediated by WhiB4 in *Mtb*.

WhiB4-mediated DNA condensation modulates redox homeostasis and survival in response to oxidative stress

Nucleoid condensation is one of the multi-layered processes exploited by bacteria to elicit oxidative stress response. For example, while Dps-mediated DNA condensation protects *S. aureus* against oxidative stress [16], *E. coli* tolerates oxidative stress primarily through OxyR-mediated changes in gene expression without altering its topology [25]. Surprisingly, to the best of our knowledge, no such correlation between nucleoid compaction and oxidative stress response exists in *Mtb*. Interestingly, recent studies have demonstrated that *E. coli* nucleoid hyper-condenses as a part of cytotoxicity induced by destructive levels of ROS generated by bactericidal antibiotics [19]. In this context, WhiB4 over-expression has recently been shown to marginally potentiate *Mtb* killing by two front-line anti-TB drugs [44]. While the mechanism behind this phenotype remained uncharacterized, it is likely that WhiB4-mediated genome compaction can result in the altered redox physiology of *Mtb* to influence drug-tolerance and oxidative stress survival. To better understand this relation, we sequentially resolved the temporal dynamics of genome compaction, cytoplasmic redox balance, and survival of *Mtb* strains upon oxidative stress (CHP treatment). We found that wt *Mtb* is able to tolerate 0.1 to 0.25 mM of CHP, whereas 0.5 to 1.0 mM CHP triggers significant killing (S7 Fig).

We performed condensation analysis on cells treated with 0.1 mM (tolerant) and 0.5 mM (lethal) of CHP over time. To correlate changes in nucleoid condensation with the internal redox state of *Mtb*, we measured the redox potential of its most abundant cytoplasmic thiol; mycothiol (MSH), using a ratiometric mycothiol biosensor, Mrx1-roGFP2 [45]. The ratiometric changes (405/488 nm) can be fitted to modified Nernst equation to precisely determine millivolt (mV) changes in the redox potential of mycothiol (E_{MSH}) [45].

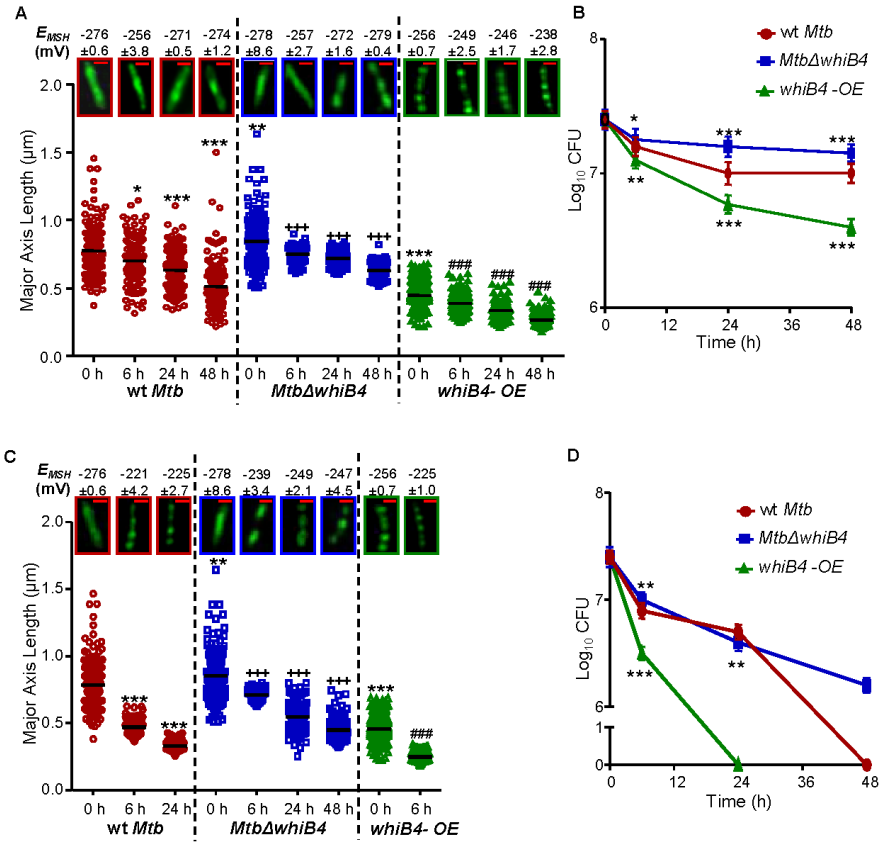

Fig. 8: Oxidative stress leads to DNA condensation, skewed redox homeostasis and bacterial killing in a WhiB4-dependent manner. wt *Mtb, MtbΔwhiB4* and *whiB4-OE* were exposed to 0.1and 0.5 mM CHP for 6, 24 and 48 h. Nucleoids of 0.1 mM **(A)** and 0.5 mM **(C)** CHP treated bacteria were stained with DAPI (pseudo colored green) and visualized by confocal microscopy (63X). The scale of images is 1µm. Major axis length of nucleoids (n=200) was measured and represented as scatter plots. Each dot represents one nucleoid. The line depicts mean of the population at each time point. P-values: * = as compared to *wt Mtb,* + = as compared to *MtbΔwhiB4,* # = as compared to *whiB4-OE* at 0 h (*P < 0.05; **P < 0.01; ***P < 0.001). E_{MSH} values, calculated for each time points using Mrx1-roGFP2, are depicted along with a corresponding image of a representative DAPI stained cell. **(B and**

D) Survival under these conditions was assessed by enumerating CFUs. Data shown is the average of experiments performed in triplicates. Error bars represent SD from the mean. P-values: * = as compared to wt *Mtb,* (*$P < 0.05$; **$P < 0.01$; ***$P < 0.001$).

Non-lethal levels of oxidative stress (0.1 mM CHP) did not induce a rapid or a significant condensation of DNA in wt *Mtb*. The average nucleoid length changed from 0.7 µm ± 0.19 to 0.63 µm ± 0.13 till 24 h post-treatment (Fig. 8A). A slightly higher condensation (0.51 ± 0.17 µm) was only evident at 48 h (Fig. 8A). The *MtbΔwhiB4* nucleoids underwent transitions similar to wt *Mtb*, although the degree of condensation was consistently lesser upon CHP treatment over time (Fig. 8A). Both wt *Mtb* and *MtbΔwhiB4* were able to maintain steady-state E_{MSH} (~-276 mV) and survival at 0.1 mM CHP, although *MtbΔwhiB4* displayed better tolerance to CHP than wt *Mtb* (Fig. 8A and 8B). Interestingly, *whiB4-OE* strain displayed marked oxidative shift in its ambient E_{MSH} (~-250 mV) without any CHP stress, indicating a relation between nucleoid condensation, WhiB4, and internal redox homeostasis in *Mtb*. Validating this observation, 0.1 mM CHP exposure intensely reduced major axis length (0.2 µM), markedly increased oxidative stress (E_{MSH} : -238 mV± 2.85), and exerted significant killing of *whiB4-OE* strain (Fig. 8A and 8B**).**

At 0.5 mM CHP, nucleoids of wt *Mtb* significantly condensed at 6h (average length: 0.46 µm ± 0.06) and 24 h (average length: 0.32 µm ± 0.04) post-treatment (Fig. 8C). At 48 h, majority of bacilli showed loss of DAPI fluorescence, appeared rounded, and irregular in shape, thus precluding any measurements of nucleoid length. These morphological alterations are indicative of DNA fragmentation and killing, which we confirmed by SYTO9 and propidium iodide staining (Fig. S8). Agreeing to above findings, 0.5 mM of CHP induced sustained oxidative stress at

each time point tested (E_{MSH} ~ -220 to -225 mV), and a complete loss of viability of wt *Mtb* at 48 h post-treatment (Fig. 8D). Notably, the skew towards condensed DNA and oxidative E_{MSH} was activated at a time point where no toxicity was observed (*i.e.* 6 h), indicating that genome hyper-compaction precedes oxidative stress induced killing of *Mtb*. Nucleoids of *MtbΔwhiB4* underwent a slower transition towards highly condensed state, which corresponds to a moderate degree of oxidative stress (E_{MSH}: -247 to -239 mV) and a relatively higher resistance to CHP stress over time (Fig. 8C and 8D). As expected, *whiB4-OE* strain was severely affected by 0.5 mM of CHP as 6 h of CHP treatment was sufficient to induce substantial DNA condensation (0.24 μm ± 0.03), overwhelm redox balance (E_{MSH} ~ -225 mV ± 0.98), and induce killing (Fig. 8C and 8D). Massive killing of *whiB4-OE* strain excluded any measurements of nucleoid major axis length at 24 and 48 h post-treatment (Fig. 8D).

Along with nucleoid compaction and killing in response to CHP stress, *whiB4-OE* strain showed proportionate increase in DNA damage and decrease in the expression of DNA repair genes as compared to wt *Mtb* and *MtbΔwhiB4* (S2 Table and S9 Fig). Lastly, the inverse correlation between DNA compaction and oxidative stress resistance was confirmed by demonstrating highly condensed nucleoids (0.4 μM axis length) of MSH deficient (*MtbΔmshA*) strain (S10 Fig). Similar to *whiB4-OE* strain, *MtbΔmshA* is also inherently sensitive to oxidative stress [46]. Altogether, these results confirm that hyper-condensation of nucleoids is associated with the lethality caused by oxidative stress in *Mtb*, and that deletion of WhiB4 reduces, and over-expression promotes, the negative impact of DNA condensation on oxidative stress survival.

Redox potential modulates WhiB4 expression and interaction with sigma factors to control genome condensation and survival

Having shown the link between oxidative stress response, genome condensation, and WhiB4, we next wanted to understand how WhiB4 can influence nucleoid condensation specifically upon oxidative stress. Using indirect immunofluorescent imaging, we found that WhiB4 formed clearly stained dots overlapping with DAPI stained nucleoids of cells displaying oxidized-E_{MSH}, indicating a direct association of WhiB4 with the condensed nucleoids (Fig. 9A). Paradoxically, qRT-PCR assays demonstrated a sequential reduction in the expression of WhiB4 with a progressive oxidative shift in E_{MSH} of *Mtb* (Fig. 9B). On initial examination, these results appear counter-intuitive. The data suggests that WhiB4 is one of the factors involved in calibrating nucleoid condensation in response to oxidative stress. The confounding observation is that oxidative stress down-regulates the expression of WhiB4. One explanation is that the repression of WhiB4 can be an elegant mycobacterial strategy to avoid killing under oxidatively hostile conditions by reducing DNA hyper-condensation and removal of its inhibitory control over oxidant-neutralizing pathways. However, the presence of WhiB4 with the oxidatively-condensed nucleoids indicate that it physically fine-tunes genome sculpture under conditions which gradually down-regulate its own expression.

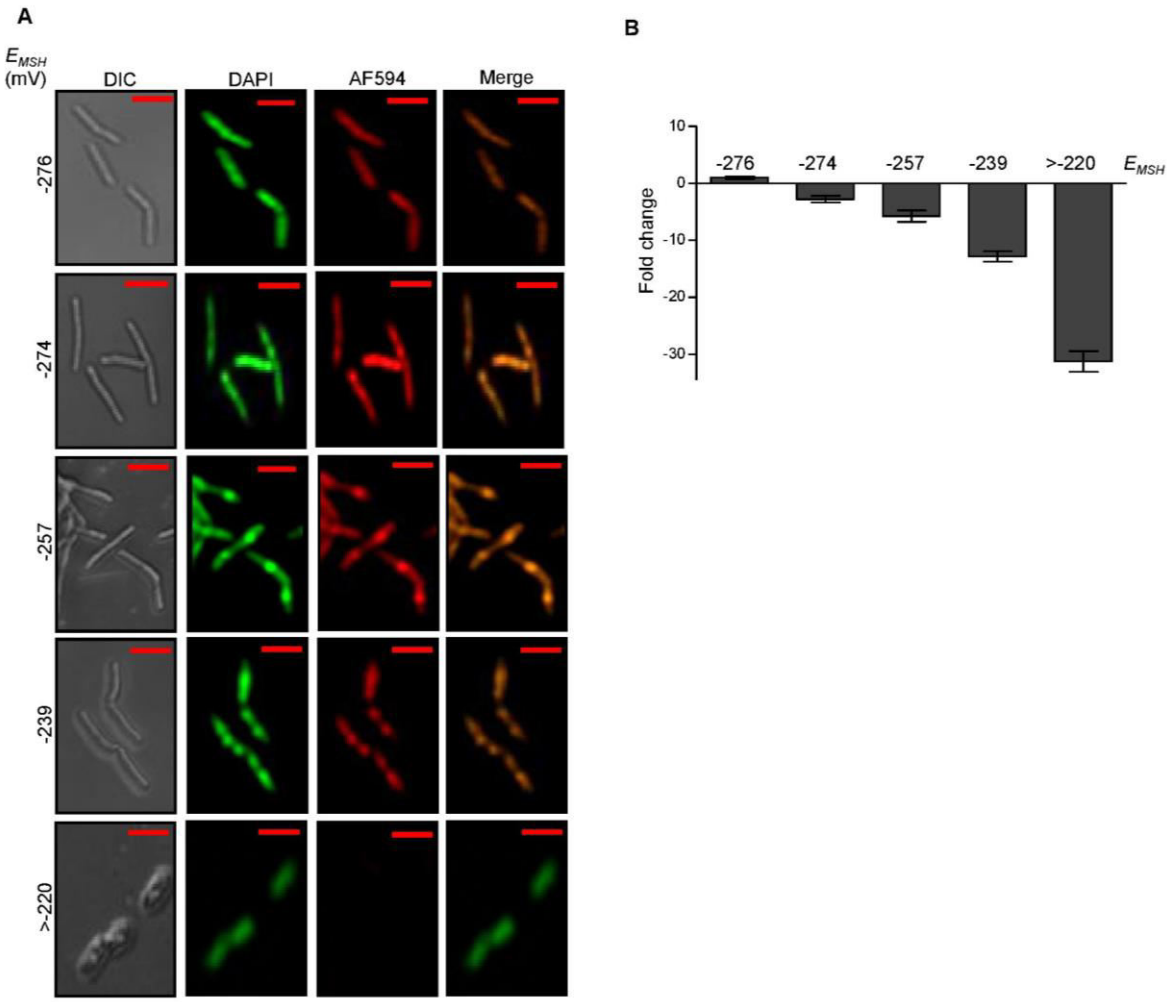

Fig. 9: **Intramycobacterial E_{MSH} modulates localization and expression of WhiB4**. **(A)** Confocal microscopic images (63X) of *MtbΔwhiB4* cells expressing histidine-tagged WhiB4 from native promoter. The intrabacterial E_{MSH} of *MtbΔwhiB4::whiB4-His* was gradually shifted towards oxidative using various concentrations of CHP. Nucleoids were stained with DAPI (pseudo colored green), WhiB4 was marked using anti- His primary antibody and AF594 conjugated secondary antibody (red), and yellow merge indicated co-localization of WhiB4 with DAPI stained nucleoids. The scale bar is 3 µm. **(B)** The wt *Mtb* displaying a range of E_{MSH} was subjected to total RNA isolation and transcription of *whiB4* was examined by qRT-PCR. Fold-change was calculated by comparing the data with untreated control. Data shown is the average of experiments performed in triplicates. Error bars represent SD from the mean.

A likely explanation comes from our earlier data showing an increase in disulfide-linked oligomerization of WhiB4 *in vivo* under oxidatuve stress (S4 Fig), which has been shown to activate DNA binding *in vitro*. The combined effect of oxidative stress on WhiB4 expression and WhiB4 oligomerization can ensure optimum intracellular concentrations of active protein required to facilitate appropriate degree of nucleoid condensation and gene expression. To understand this mechanism, we examined homo-dimerization of WhiB4 inside mycobacteria under defined oxidative and reductive conditions using mycobacterial-protein fragment complementation (M-PFC) [47]. The M-PFC system works on the principle that murine dihydrofolate reductase (mDHFR) complementary fragments [F1,2] and [F3] can be functionally re-constituted via interaction between two interacting proteins in *Msm*, which increases bacterial resistance to trimethoprim (TRIM).

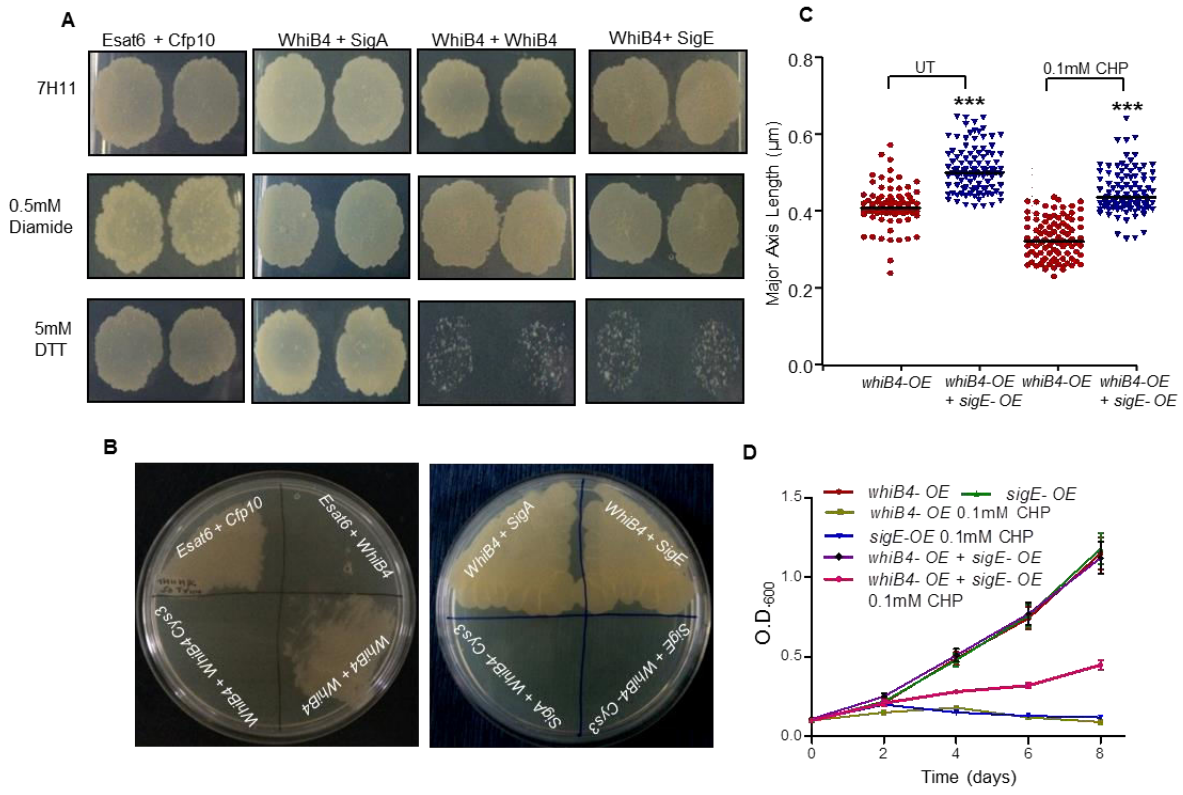

Fig.10: Redox-dependent homo-dimerization and hetero-dimerization of WhiB4 with SigA and SigE. (A) *Msm* cells expressing protein-DHFR fusion fragments were scored for WhiB4:WhiB4, WhiB4:SigA and WhiB4:SigE interactions by plating in the presence of trimethoprim (TRIM). Interactions were also examined in the presence of altered redox environment using 0.5 mM diamide (oxidant) or 5 mM DTT (reductant). **(B)** Redox-dependent interaction of WhiB4 was confirmed by examining the interaction with the WhiB4-Cys3 variant. Positive and negative controls include Esat6:Cfp10 and Esat6:WhiB4 interactions, respectively. **(C)** Nucleoid of *Msm* over-expressing WhiB4 and SigE from tetracycline inducible and *hsp60* promoter, respectively, under unstressed or CHP stressed conditions were stained with DAPI (pseudo colored green) and visualized by confocal microscopy (63X). Major axis length of nucleoids (n=200) was measured and represented as scatter plots. Each dot represents one nucleoid. The line depicts mean of the population at each time point. . P-values: * = as compared to *whiB4-OE* (***P < 0.001). **(D)** Growth of *Msm* strains either independently over-expressing or co-expressing WhiB4 and SigE under normal conditions or in presence of 0.1 mM CHP. Data shown is the average of two experiments performed in triplicates. Error bars represent SD from the mean.

The WhiB4 monomers were co-expressed as fusion partners of DHFR fragments ([F1,2] and [F3]) in *Msm* and strength of interaction was examined by monitoring the extent of growth on media containing TRIM [47]. To understand the influence of oxidative stress on WhiB4:WhiB4 association, we altered the E_{MSH} of *Msm* strain co-expressing WhiB4-[F1,2] and WhiB4-[F3] fusions to oxidative (>-220 mV) or reductive (<-320 mV) using cell-permeable thiol-oxidant (diamide; 0.5 mM) or thiol-reductant (DTT; 5 mM), respectively. Growth on TRIM was readily detected in case of *Msm* expressing WhiB4-[F1,2] and WhiB4-[F3] fusions, confirming homo-dimerization of WhiB4 under normal growing conditions (Fig. 10A). No interaction of WhiB4 was observed with an unrelated mycobacterial protein, Esat-6, confirming the specificity of interaction (Fig. 10B). Importantly, treatment with diamide demonstrated a robust growth of *Msm* expressing WhiB4-[F1,2] and WhiB4-[F3] fusions on TRIM,

indicating a stronger interaction, whereas DTT virtually abolished the growth on TRIM (Fig. 10A). Exposure to DTT/diamide did not alter interaction between other mycobacterial proteins *i.e.* Esat-6 and Cfp10 (Fig. 10A). Furthermore, replacement of a redox-active cysteine residue (Cys3) with alanine in WhiB4 (WhiB4-cys3) abolished WhiB4 dimerization (Fig. 10B), confirming the role of thiol-disulfide switch in driving the interaction (Fig. 10B).

WhiB proteins can act as transcription factors by making physical contact with SigA [32, 33]. Further, a new finding shows that WhiBs interaction with SigA could be one of the mechanisms regulating thier monomeric state and transcription regulatory function [48]. We reasoned that WhiB4-SigA interaction may provide an additional control over WhiB4 self-association and subsequent genome condensation upon oxidative stress. However, WhiB4-SigA interaction displayed insensitivity towards oxidative or reductive stress (Fig. 10A). Since, our network analysis captured SigB, SigE, and SigH as major hub nodes activated in *MtbΔwhiB4* upon oxidative stress, we explored interaction of these sigma factors with WhiB4. While interaction of WhiB4 was very weak and redox-independent with SigB and SigH (data not shown), a strong and redox-dependent association was detected with SigE (Fig 10A). No interaction was found between SigE and WhiB4-cys3 variant (Fig. 10B). Interestingly, over-expression of SigE in *whiB4-OE* to some extent relieved the negative impact of WhiB4 over-expression on genome condensation (Fig. 10C) and toxicity in response to CHP challenge (Fig. 10D), indicating a physiological role of SigE-WhiB4 association in controlling nucleoid compaction, gene expression, and survival under oxidative stress.

WhiB4 over-expression reduces mycobacterial survival *in vivo*

It can be argued that over-expression of WhiB4 can have a generalized effect on gene expression and survival in response to multiple stresses. However, our qRT-PCR data confirmed the impact of over-expression was specific on genes regulated by WhiB4 (S2 Table). In line with this, we discovered that WhiB4 over-expression does not compromise mycobacterial survival under normal growth conditions or upon exposure to other stresses such as acid and heat, indicating that the bactericidal effect is likely to be specific to oxidative stress (S11 Fig). Agreeing to this, *whiB4-OE* strain exhibited greater death as compared to wt *Mtb* and *MtbΔwhiB4* inside the oxidatively hostile-environment of RAW 264.7 macrophages activated by IFN-ɣ and LPS (Fig. 11A). Inhibition of iNOS using N^G-Methyl-L-Arginine (NMLA) restored the survival defect of *whiB4-OE* strain (Fig. 11B). Furthermore, a significantly higher fraction of *whiB4-OE* cells displayed E_{MSH}-oxidized inside activated RAW 264.7 macrophages as compared to wt *Mtb* and *MtbΔwhiB4* (S12 Fig). Lastly, we assessed if over-expression of WhiB4 affected growth of *Mtb in vivo*. We were concerned that a low dose aerosol infection may diminish the survival of *whiB4-OE* strain to an extent where it is difficult for us to recover bacteria from the infected organs. Therefore, we measured survival kinetics in the acute murine model of TB infection. Approximately 3.5 $\log_{10}$ of CFUs of wt *Mtb* and *whiB4-OE* strain were implanted in the lungs of three groups of immuno-competent BALB/c mice (Fig. 11C).

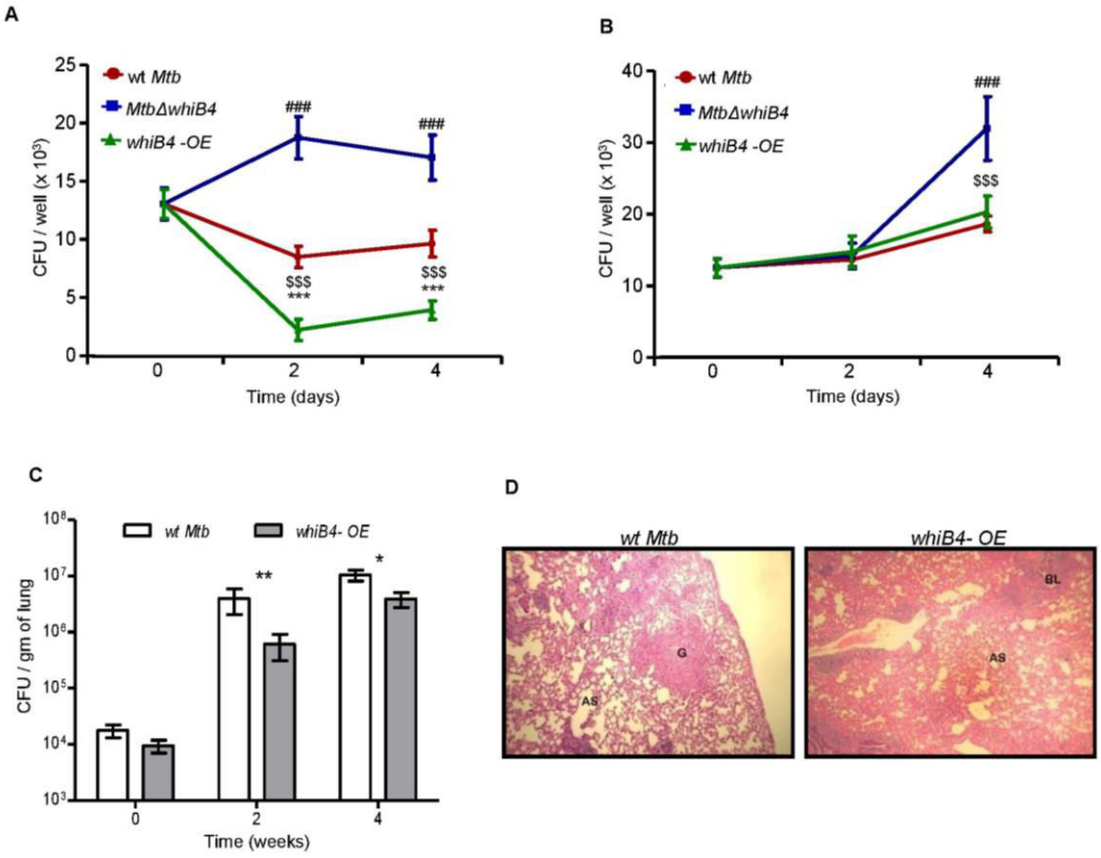

Fig. 11: WhiB4 over-expression reduces mycobacterial survival *in vivo.* (A) IFN-ɣ-LPS activated RAW 264.7 macrophages were infected with wt *Mtb*, *MtbΔwhiB4* and *whiB4-OE* strains and survival was monitored by enumerating CFU. **(B)** Inhibition of NO using iNOS inhibitor (NMLA) significantly rescued the killing *whiB4-OE*. The data is shown as Mean (± SD) from two independent experiments having triplicate wells each. P-values: # = *MtbΔwhiB4* vs. wt *Mtb*, $ = *whiB4- OE* vs. *MtbΔwhiB4*, and * = *whiB4- OE* vs. wt *Mtb* (*P < 0.05; **P < 0.01; ***P < 0.001). **(C)** BALB/c mice were infected by aerosol and survival of various strains was monitored at 2 and 4 weeks' time post infection in lungs. Error bars represent SD from the mean. **(D)** Lungs section from mice infected with wt *Mtb* and *whiB4-OE* strains. The histopathological analysis showed granuloma formation in the wt *Mtb* strain as compared to the *whiB4-OE* strain. All images were taken at 40X magnification.

The *whiB4-OE* strain showed clear growth attenuation in the lungs of animals. Also, the lungs of mice infected with the *whiB4-OE* strain showed increased cellular infiltration and tissue damage (Fig 11D). Taken together, we conclude that WhiB4 is

a virulence regulatory protein that fine tunes the response to oxidative stress by adjusting nucleoid condensation and expression of oxidative stress responsive modules (possibly through interaction with sigma factors) to maintain redox homeostasis.

Discussion

In this study, we identified a link between DNA condensation, WhiB4, internal redox balance, and oxidative stress response in *Mtb*. By integrating computational and experimental approaches, we generated a highly resolved view of activities differentially regulated by oxidative stress in a WhiB4-specific manner in *Mtb.* Other than general stress-response pathways, we identified DnaK chaperone as a major hub node moderating oxidative stress response in *Mtb*. Validating our analysis, two recent studies have suggested the importance of DnaK-ClpB network in sequestering irreversibly oxidized proteins to promote recovery from oxidative stress [49, 50]. Loss of WhiB4 resulted in hyper-activation of pathways encoding antioxidants, CCM, DNA repair and virulence regulators upon CHP stress. We identified that the redox-mediated association of WhiB4 with SigE can be central to WhiB4 coordinated oxidative stress response in *Mtb*. On this basis, we propose that WhiB4 with nucleoid condensing activity mediates a large scale influence on chromosomal architecture to provide a regulatory background for precise activation or repression of stress genes by sequence-specific transcription and/or sigma factors. Establishing how WhiB4 works in conjunction with specific transcriptional regulators is an area of further experimentation. Altogether, WhiB4 is required to

ensure appropriate degree of genome condensation and proper expression of oxidative stress responsive genes in *Mtb*.

WhiB proteins are proposed to be Fe-S cluster containing transcription factors, however, exact molecular mechanism remained poorly understood. Studies revealed that some of the WhiB family members might regulate gene expression by binding to AT- or GC- rich regions rather than specific DNA sequences [20, 36, 51]. Furthermore, ChIP-Seq analysis of WhiB in *Sco* seems to indicate a non-sequence specific DNA binding wherein a specific regulatory effect may be achieved by its association with WhiA [35]. Exploiting various experimental approaches, we confirmed that WhiB4 condenses DNA in a sequence-independent, but redox-dependent manner. A modest influence of WhiB4 on nucleoid condensation under normal growing conditions could be due to a compensatory role of other NAPs such as Lsr2, EspR, and HupB in controlling genome architecture. In line with this, over-expression of WhiB4 induced hyper-condensation of nucleoids *in vivo*, indicating that the protein, in sufficient quantity, can function independently in regulating DNA compaction. Of note, over-expression of NAPs (*e.g*. Dps) does not always result in nucleoid condensation owing to negative influence of other NAPs (*e.g*. Fis) [25]. While over-expression of WhiB4 alone can condense nucleoid *in vivo*, how it contributes to DNA condensation in conjunction with other mycobacterial NAPs at physiological concentrations, remains to be determined.

A major phenotype of *MtbΔwhiB4* is its elevated ability to tolerate oxidative stress. We not only observed a significant complementation of this phenotype upon

over-expression of WhiB4, but also observed hyper-sensitivity of *whiB4-OE* strain to oxidative stress *in vitro*, inside macrophages, and *in vivo*. These observations provide a link between DNA condensation, oxidative stress response, and virulence in *Mtb*. Several NAPs are known to play an important role in influencing nucleoid condensation under specific stress conditions such as iron starvation, hypoxia, and acidic pH [13]. However, the importance of DNA condensation and NAPs in controlling oxidative stress response remains controversial. Notably similar to WhiB4, several *in vitro* studies have clearly indicated that NAPs (*e.g*. Lsr2 and Dps) generally provide physical barrier to protect DNA against oxidative stress [14, 15]. However, whether this is relevant *in vivo* is not well-defined. For example, while *S. aureus* resists H_2O_2 by rapidly condensing DNA through a Dps homolog (MrgA)[16], oxidative stress simply did not lead to DNA condensation in other bacteria including *Streptomyces*, *Dickeya dadantii*, and *E. coli* [25, 52, 53]. Interestingly, a recent study elegantly showed that MrgA-mediated protection of *S. aureus* from oxidative stress is mainly due to its ferroxidase activity rather than its ability to shield DNA [54]. Lastly, the role of Lsr2 in protecting *Mtb* from oxidative damage by shielding DNA is controversial [15, 55]. Therefore, it is unclear as yet how mycobacteria remodel their DNA condensation during oxidative stress.

To begin understanding this, we demonstrated that non-toxic levels of oxidative stress neither induce a rapid nor a significant degree of nucleoid condensation in *Mtb*. In contrast, toxic levels of oxidative stress rapidly induced DNA condensation. WhiB4 seems to be involved in regulating DNA condensation under both of these conditions. Loss of WhiB4 delays DNA condensation, maintains redox homeostasis, and protects cells from oxidative stress, whereas over-expression

reversed these phenotypes. While our expression and redox potential data indicates that the detrimental effect of WhiB4 over-expression and oxidative stress is likely due to repression of antioxidant machinery and diminished capacity to counteract cytoplasmic redox stress, it is possible that hyper-condensation of nucleoid may have inhibited other metabolic processes such as DNA replication/repair, transcription, and translation to exert efficient killing. In line with this, we observed a dramatic repression of topology modifying genes and DNA repair genes in WhiB4 over-expressing strain upon oxidative stress. Hence, we conclude that resistance to oxidative stress is unlikely mediated by nucleoid compaction in *Mtb*. In this context, it has been suggested that certain bacteria (gamma-proteobacteria) have evolved genetic mechanisms (*e.g.* Fis, TopA, and GyrA) to block DNA condensation and promote the expression of OxyR dependent antioxidant genes as a major mechanism to guard genomic DNA against oxidative stress [25]. Moreover, similar to *Mtb*, toxic levels of oxidative stress mediate killing of *E. coli* by inducing a long lasting nucleoid condensation [19, 56]. Although, unlike *Mtb,* where WhiB4 over-expression is sufficient to induce both DNA condensation and killing, a similar consequence of oxidative stress seems to be mediated through a combined action of multiple OxyR-regulated NAPs including H-NS, Hup, Him, MukB, and Dps in *E.coli* [19]. In the absence of OxyR, Fis and Dps activities, WhiB4 can be an important regulator of both nucleoid condensation and expression of oxidative stress responsive genes in *Mtb*. We propose that under unstressed conditions, limited oxidation of WhiB4 activates DNA binding and ensures appropriate degree of nucleoid condensation to preclude unnecessary expression of oxidative stress responsive pathways. Down-regulation of WhiB4 expression along with its homo-dimerization under oxidative stress conditions gradually regulates WhiB4 condensing

activity to alleviate the negative impact of nucleoid hyper-condensation and fine tunes the induction of antioxidant pathways via interaction with sigma factors. Both of these activities ensure optimum tolerance to oxidative stress. We have recently shown that while *Mtb* is genetically equipped to dissipate exogenous oxidative stress via secretion of several oxidant remediation systems, endogenous increase in ROS is a potent inducer of death [8]. Therefore, while a certain degree of oxidative stress can be efficiently mitigated by secretory antioxidants, including those in *whiB4*-regulon, without posing a risk for internal targets such as DNA; sustained levels of oxidative stress that exceeds defence capabilities can damage DNA. Under these conditions a rapid increase in hyper-condensation via WhiB4 and/or other NAPs may provide a programmed mechanism to mark and trigger death of severely stressed cells. This process may be highly relevant to infection conditions where host environment triggers a gradient of oxidative stress within *Mtb* population [45].

Lastly, it is worthwhile to note that nucleoid condensation and cessation of DNA replication is a part of sporulation program triggered by Wbl proteins in response to environmental signal(s) in *Streptomyces coelicolor* (*Sco*) [57] . In fact, *whiA* and *whiB* mutants of *Sco* also exhibit uncondensed nucleoid in their aerial hyphae resulting in sporulation defects [57]. Our results raised an interesting possibility of Wbl proteins as a direct mediator of genome condensation in actinomycetes during sporulation, thus invoking a broad significance. Recently, dynamic changes in mycobacterial nucleoid content and structure upon nutrient starvation were shown to trigger a development program resulting in the formation of a small-cell morphotype with elevated antibiotic tolerance and persistence capablities [58]. Since WhiB4 expression is induced in response to hypoxia and

nutrient starvation [59, 60], it is reasonable to propose that WhiB4-directed nucleoid hyper-condensation might mediate development and differentiation in *Mtb* under dormancy inducing conditions for long term persistence (currently under progress). In conclusion, the combined results indicate that WhiB4 is a candidate for a dual-function NAP that could integrate environmental signals with DNA conformation and transcription. The focus of present investigations has been mainly on the nucleoid condensing function of WhiB4 and how it can modulate oxidative stress response in *Mtb*. As far as we are aware, this is the first example of a redox-dependent NAP in bacteria.

Materials and Methods

Bacterial strains and growth conditions

Wt *Mtb*, *Mtb*Δ*whiB4* and *whiB4-OE* strains were cultivated as described [20]. *E. coli* cultures were grown in Luria-Bertani (LB) medium (BD Biosciences). When required, culture medium was supplemented with hygromycin (50 μg/ml for mycobacteria, 150 μg/ml for *E.coli*), kanamycin (25 μg/ml), and ampicillin (100 μg/ml). For cumene hydroperoxide (CHP, Sigma Aldrich) stress, strains were grown to an exponential phase and exposed to 0.1, 0.25, 0.5 and 1 mM CHP. Survival was monitored by enumerating colony forming units at 0, 6, 24, and 48 h post-treatment. To examine the generalized influence of WhiB4 over-expression on stress tolerance, *whiB4-OE* strain was grown aerobically till $O.D._{600}$ of 0.3, induced with 200 ng/ml Anhydro Tetracycline (ATc, Cayman Chemicals) for 24 h at 37^{o}C, and exposed to (i) normal aerobic environment, (ii) acidic stress (pH 4.5), and (iii) heat stress (42^{o}C). The growth kinetics was monitored over time by measuring absorbance at 600 nm.

Microarray experiments and Network Construction

The wt *Mtb* and *MtbΔwhiB4* strains were grown to an $O.D._{600}$ of 0.3-0.4 and exposed to 0.25 mM CHP for 2 h at 37^{o}C. Total RNA was isolated, processed, and hybridized to *Mtb* Whole Genome Gene Expression Profiling microarray- G2509F (AMADID: G2509F_034585, Agilent Technologies PLC) and data was analyzed as described [61]. The normalized data has been submitted to NCBI's Gene Expression Omnibus (GEO, http://www.ncbi.nlm.nih.gov/geo/); accession number GSE73877. For network construction please see S1 Note.

Electrophoretic Mobility Shift Assays (EMSA)

Histidine-tagged version of WhiB4 and its various cysteine mutants were purified by as described previously [20]. Oxidized apo-form of WhiB4 was prepared as described [20]. For EMSA assays, intragenic DNA fragments and promoter fragments (~200 bp upstream of the translational start codon) were amplified using specific oligonucleotides (Table S6), radio-labeled, and EMSAs were performed as described previously [20]. For non-specific DNA binding ability of WhiB4, oxidized apo-WhiB4 was incubated with various DNA molecules in a buffer containing 89 mM Tris, 89 mM boric acid and 1 mM EDTA (pH 8.4) for 30 min. The protein-DNA complexes were resolved on a 1% agarose gel in 1x TBE buffer, stained with ethidium bromide and visualized under UV light.

In vitro transcription assays

Approximately 350 ng of oxidized apo-WhiB4 was incubated with 150 ng of pGEM plasmid in a final volume of 20 µl, followed by *in vitro* transcription using the Riboprobe *in vitro* Transcription Kit according to the manufacturer's instructions (Promega). Samples were treated with 6% SDS (Amresco Inc.) and 4 mg/ml proteinase K (Amresco Inc.) for 30 min at 37^{o}C and reaction products were analyzed on a 1% agarose gel.

DNase I protection assay and Fenton-mediated damage

The oxidized apo-WhiB4 was incubated with pCV125 plasmid DNA for 30 min. This was followed by treatment of the protein:DNA complex by 1 unit of DNase I (Thermo Scientific) or 100 µM $FeSO_4$ (Amresco Inc.) plus 10 mM H_2O_2 (MP Biomedicals). The reaction mixture was incubated at 37^{o}C for 1 min for DNase I treatment and 30 min for assessing Fenton damage. This was followed by inactivation of DNase I at 75^{o}C for 10 min and degradation of WhiB4 by 6% SDS and 4 mg/ml protease K (Thermo Scientific) for 30 min at 37^{o}C. The remaining samples were checked for the extent of DNA degradation by analyzing on a 1% agarose gel.

Atomic force microscopy (AFM)

The oxidized apo-WhiB4 was incubated with 7ng/ µl of supercoiled or relaxed forms of plasmid DNA (pCV125) in a concentration range from 1:2 to 1:8 (DNA: WhiB4; w/w) at RT and 10µl of this solution was loaded onto freshly cleaved mica surface. Similar, procedure was followed for Cys3-WhiB4 following incubation with DNA at RT. The 10µl of protein-DNA mix was allowed to spread spontaneously and incubated for 1 min to allow molecules to adhere on mica surface. The unbound

material was washed with deionised water and the bound surface allowed to air dry. Imaging was carried out with 5500 scanning probe microscope (Agilent Technologies, Inc.) using PicoView software. Images were obtained in tapping mode in air with 225-mm-long silicon cantilevers (Agilent Technologies) that have a resonance frequency of 75 kHz and a force constant of 2.8 Newton/m. Scan speed used was 1 line/s. Minimum image processing (first order flattening and brightness contrast) was employed. Image analysis was performed using Pico Image software v1.4.4.

E_{MSH} measurements

Measurements of intrabacterial E_{MSH} during growth *in vitro*, upon exposure to CHP stress, and inside immune-activated RAW 264.7 were done as described previously [45].

Miscellaneous procedures

Additional materials and methods are provided in the supporting information.

Ethics Statement

This study was carried out in strict accordance with the guidelines provided by the Committee for the Purpose of Control and Supervision on Experiments on Animals (CPCSEA), Government of India. The protocol was approved by the Committee of the International Centre for Genetic Engineering and Biotechnology, New Delhi, India (Approval number: ICGEB/AH/2011/2/IMM-26). All efforts were made to minimize the suffering.

Acknowledgements

We are thankful to the University of Delhi South Campus MicroArray Centre (UDSCMAC), New Delhi, for conducting microarray experiment. We thank IISc and ICCGEB for providing BSL3 facilities. We are also grateful to Imaging Facility at University of Delhi, South Campus, New Delhi, for all the confocal microscopy experiments and analysis. We are thankful to N. Ganesh, Department of Biochemistry, IISc, Bangalore, and Anjana Badrinarayanan, Massachusetts Institute of Technology, USA, for their comments and feedback.

References

1. Ehrt S, Schnappinger D. Mycobacterial survival strategies in the phagosome: defence against host stresses. Cell Microbiol. 2009;11(8):1170-8. Epub 2009/05/15. doi: 10.1111/j.1462-5822.2009.01335.x. PubMed PMID: 19438516; PubMed Central PMCID: PMC3170014.

2. Sato K, Akaki T, Tomioka H. Differential potentiation of anti-mycobacterial activity and reactive nitrogen intermediate-producing ability of murine peritoneal macrophages activated by interferon-gamma (IFN-gamma) and tumour necrosis factor-alpha (TNF-alpha). Clin Exp Immunol. 1998;112(1):63-8. Epub 1998/05/05. PubMed PMID: 9566791; PubMed Central PMCID: PMC1904942.

3. Cooper AM, Segal BH, Frank AA, Holland SM, Orme IM. Transient loss of resistance to pulmonary tuberculosis in p47(phox-/-) mice. Infect Immun. 2000;68(3):1231-4. Epub 2000/02/26. PubMed PMID: 10678931; PubMed Central PMCID: PMC97272.

4. MacMicking J, Xie QW, Nathan C. Nitric oxide and macrophage function. Annu Rev Immunol. 1997;15:323-50. Epub 1997/01/01. doi: 10.1146/annurev.immunol.15.1.323. PubMed PMID: 9143691.

5. Ng VH, Cox JS, Sousa AO, MacMicking JD, McKinney JD. Role of KatG catalase-peroxidase in mycobacterial pathogenesis: countering the phagocyte oxidative burst. Mol Microbiol. 2004;52(5):1291-302. PubMed PMID: 15165233.

6. Yang CT, Cambier CJ, Davis JM, Hall CJ, Crosier PS, Ramakrishnan L. Neutrophils exert protection in the early tuberculous granuloma by oxidative killing of mycobacteria phagocytosed from infected macrophages. Cell Host Microbe.

2012;12(3):301-12. Epub 2012/09/18. doi: 10.1016/j.chom.2012.07.009. PubMed PMID: 22980327; PubMed Central PMCID: PMC3638950.

7. Lee PP, Chan KW, Jiang L, Chen T, Li C, Lee TL, et al. Susceptibility to mycobacterial infections in children with X-linked chronic granulomatous disease: a review of 17 patients living in a region endemic for tuberculosis. Pediatr Infect Dis J. 2008;27(3):224-30. Epub 2008/02/19. doi: 10.1097/INF.0b013e31815b494c. PubMed PMID: 18277931.

8. Tyagi P, Dharmaraja AT, Bhaskar A, Chakrapani H, Singh A. *Mycobacterium tuberculosis* has diminished capacity to counteract redox stress induced by elevated levels of endogenous superoxide. Free Radic Biol Med. 2015;84:344-54. Epub 2015/03/31. doi: 10.1016/j.freeradbiomed.2015.03.008. PubMed PMID: 25819161; PubMed Central PMCID: PMC4459714.

9. Kumar A, Farhana A, Guidry L, Saini V, Hondalus M, Steyn AJ. Redox homeostasis in mycobacteria: the key to tuberculosis control? Expert Rev Mol Med. 2011;13:e39. Epub 2011/12/17. doi: 10.1017/S1462399411002079. PubMed PMID: 22172201; PubMed Central PMCID: PMC3241215.

10. Nambi S, Long JE, Mishra BB, Baker R, Murphy KC, Olive AJ, et al. The Oxidative Stress Network of *Mycobacterium tuberculosis* Reveals Coordination between Radical Detoxification Systems. Cell Host Microbe. 2015;17(6):829-37. Epub 2015/06/13. doi: 10.1016/j.chom.2015.05.008. PubMed PMID: 26067605; PubMed Central PMCID: PMC4465913.

11. Buchmeier NA, Newton GL, Fahey RC. A mycothiol synthase mutant of *Mycobacterium tuberculosis* has an altered thiol-disulfide content and limited tolerance to stress. J Bacteriol. 2006;188(17):6245-52. Epub 2006/08/23. doi:

10.1128/JB.00393-06. PubMed PMID: 16923891; PubMed Central PMCID: PMC1595396.

12. Genghof DS, Vandamme O. Biosynthesis of Ergothioneine and Hercynine by Mycobacteria. Journal of bacteriology. 1964;87:852-62. PubMed PMID: 14137624; PubMed Central PMCID: PMCPMC277104.

13. Dillon SC, Dorman CJ. Bacterial nucleoid-associated proteins, nucleoid structure and gene expression. Nat Rev Microbiol. 2010;8(3):185-95. Epub 2010/02/09. doi: 10.1038/nrmicro2261. PubMed PMID: 20140026.

14. Martinez A, Kolter R. Protection of DNA during oxidative stress by the nonspecific DNA-binding protein Dps. Journal of bacteriology. 1997;179(16):5188-94. PubMed PMID: 9260963; PubMed Central PMCID: PMCPMC179379.

15. Colangeli R, Haq A, Arcus VL, Summers E, Magliozzo RS, McBride A, et al. The multifunctional histone-like protein Lsr2 protects mycobacteria against reactive oxygen intermediates. Proc Natl Acad Sci U S A. 2009;106(11):4414-8. Epub 2009/02/25. doi: 10.1073/pnas.0810126106. PubMed PMID: 19237572; PubMed Central PMCID: PMC2657463.

16. Morikawa K, Ohniwa RL, Kim J, Maruyama A, Ohta T, Takeyasu K. Bacterial nucleoid dynamics: oxidative stress response in *Staphylococcus aureus.* Genes Cells. 2006;11(4):409-23. doi: 10.1111/j.1365-2443.2006.00949.x. PubMed PMID: 16611244.

17. Weinstein-Fischer D, Elgrably-Weiss M, Altuvia S. *Escherichia coli* response to hydrogen peroxide: a role for DNA supercoiling, topoisomerase I and Fis. Molecular microbiology. 2000;35(6):1413-20. PubMed PMID: 10760142.

18. Wang H, Wang F, Hua X, Ma T, Chen J, Xu X, et al. Genetic and biochemical characteristics of the histone-like protein DR0199 in *Deinococcus radiodurans*.

Microbiology. 2012;158(Pt 4):936-43. doi: 10.1099/mic.0.053702-0. PubMed PMID: 22282513.

19. Ko KC, Tai PC, Derby CD. Mechanisms of action of escapin, a bactericidal agent in the ink secretion of the sea hare Aplysia californica: rapid and long-lasting DNA condensation and involvement of the OxyR-regulated oxidative stress pathway. Antimicrobial agents and chemotherapy. 2012;56(4):1725-34. doi: 10.1128/AAC.05874-11. PubMed PMID: 22232273; PubMed Central PMCID: PMCPMC3318362.

20. Chawla M, Parikh P, Saxena A, Munshi M, Mehta M, Mai D, et al. *Mycobacterium tuberculosis* WhiB4 regulates oxidative stress response to modulate survival and dissemination in vivo. Mol Microbiol. 2012;85(6):1148-65. Epub 2012/07/12. doi: 10.1111/j.1365-2958.2012.08165.x. PubMed PMID: 22780904; PubMed Central PMCID: PMC3438311.

21. den Hengst CD, Buttner MJ. Redox control in actinobacteria. Biochim Biophys Acta. 2008;1780(11):1201-16. PubMed PMID: 18252205.

22. Mehta M, Rajmani RS, Singh A. *Mycobacterium tuberculosis* WhiB3 Responds to Vacuolar pH-induced Changes in Mycothiol Redox Potential to Modulate Phagosomal Maturation and Virulence. J Biol Chem. 2016;291(6):2888-903. Epub 2015/12/08. doi: 10.1074/jbc.M115.684597. PubMed PMID: 26637353; PubMed Central PMCID: PMC4742752.

23. Sambarey A, Prashanthi K, Chandra N. Mining large-scale response networks reveals 'topmost activities' in *Mycobacterium tuberculosis* infection. Sci Rep. 2013;3:2302. doi: 10.1038/srep02302. PubMed PMID: 23892477; PubMed Central PMCID: PMCPMC3725478.

24. Hegde SR, Rajasingh H, Das C, Mande SS, Mande SC. Understanding communication signals during mycobacterial latency through predicted genome-wide protein interactions and boolean modeling. PloS one. 2012;7(3):e33893. doi: 10.1371/journal.pone.0033893. PubMed PMID: 22448278; PubMed Central PMCID: PMCPMC3309013.

25. Ohniwa RL, Morikawa K, Kim J, Ohta T, Ishihama A, Wada C, et al. Dynamic state of DNA topology is essential for genome condensation in bacteria. EMBO J. 2006;25(23):5591-602. doi: 10.1038/sj.emboj.7601414. PubMed PMID: 17093499; PubMed Central PMCID: PMCPMC1679767.

26. Schneider R, Travers A, Kutateladze T, Muskhelishvili G. A DNA architectural protein couples cellular physiology and DNA topology in *Escherichia coli*. Mol Microbiol. 1999;34(5):953-64. PubMed PMID: 10594821.

27. Tian J, Bryk R, Shi S, Erdjument-Bromage H, Tempst P, Nathan C. *Mycobacterium tuberculosis* appears to lack alpha-ketoglutarate dehydrogenase and encodes pyruvate dehydrogenase in widely separated genes. Mol Microbiol. 2005;57(3):859-68. doi: 10.1111/j.1365-2958.2005.04741.x. PubMed PMID: 16045627.

28. Shi S, Ehrt S. Dihydrolipoamide acyltransferase is critical for *Mycobacterium tuberculosis* pathogenesis. Infect Immun. 2006;74(1):56-63. doi: 10.1128/IAI.74.1.56-63.2006. PubMed PMID: 16368957; PubMed Central PMCID: PMCPMC1346611.

29. Maksymiuk C, Balakrishnan A, Bryk R, Rhee KY, Nathan CF. E1 of alpha-ketoglutarate dehydrogenase defends *Mycobacterium tuberculosis* against glutamate anaplerosis and nitroxidative stress. Proc Natl Acad Sci U S A.

2015;112(43):E5834-43. Epub 2015/10/03. doi: 10.1073/pnas.1510932112. PubMed PMID: 26430237; PubMed Central PMCID: PMC4629369.

30. Venugopal A, Bryk R, Shi S, Rhee K, Rath P, Schnappinger D, et al. Virulence of *Mycobacterium tuberculosis* depends on lipoamide dehydrogenase, a member of three multienzyme complexes. Cell Host Microbe. 2011;9(1):21-31. Epub 2011/01/18. doi: 10.1016/j.chom.2010.12.004. PubMed PMID: 21238944; PubMed Central PMCID: PMC3040420.

31. Houghton J, Townsend C, Williams AR, Rodgers A, Rand L, Walker KB, et al. Important role for *Mycobacterium tuberculosis* UvrD1 in pathogenesis and persistence apart from its function in nucleotide excision repair. J Bacteriol. 2012;194(11):2916-23. doi: 10.1128/JB.06654-11. PubMed PMID: 22467787; PubMed Central PMCID: PMCPMC3370636.

32. Steyn AJ, Collins DM, Hondalus MK, Jacobs WR, Jr., Kawakami RP, Bloom BR. *Mycobacterium tuberculosis* WhiB3 interacts with RpoV to affect host survival but is dispensable for in vivo growth. Proc Natl Acad Sci U S A. 2002;99(5):3147-52. PubMed PMID: 11880648.

33. Burian J, Yim G, Hsing M, Axerio-Cilies P, Cherkasov A, Spiegelman GB, et al. The mycobacterial antibiotic resistance determinant WhiB7 acts as a transcriptional activator by binding the primary sigma factor SigA (RpoV). Nucleic Acids Res. 2013;41(22):10062-76. Epub 2013/08/31. doi: 10.1093/nar/gkt751. PubMed PMID: 23990327; PubMed Central PMCID: PMC3905903.

34. Soliveri JA, Gomez J, Bishai WR, Chater KF. Multiple paralogous genes related to the Streptomyces coelicolor developmental regulatory gene whiB are present in Streptomyces and other actinomycetes. Microbiology. 2000;146 (Pt 2):333-43. doi: 10.1099/00221287-146-2-333. PubMed PMID: 10708372.

35. Bush MJ, Chandra G, Bibb MJ, Findlay KC, Buttner MJ. Genome-Wide Chromatin Immunoprecipitation Sequencing Analysis Shows that WhiB Is a Transcription Factor That Cocontrols Its Regulon with WhiA To Initiate Developmental Cell Division in *Streptomyces*. MBio. 2016;7(2). doi: 10.1128/mBio.00523-16. PubMed PMID: 27094333; PubMed Central PMCID: PMCPMC4850268.

36. Singh A, Crossman DK, Mai D, Guidry L, Voskuil MI, Renfrow MB, et al. *Mycobacterium tuberculosis* WhiB3 maintains redox homeostasis by regulating virulence lipid anabolism to modulate macrophage response. PLoS Pathog. 2009;5(8):e1000545. PubMed PMID: 19680450.

37. Smith LJ, Stapleton MR, Fullstone GJ, Crack JC, Thomson AJ, Le Brun NE, et al. *Mycobacterium tuberculosis* WhiB1 is an essential DNA-binding protein with a nitric oxide-sensitive iron-sulfur cluster. Biochem J. 2010;432(3):417-27. Epub 2010/10/12. doi: 10.1042/BJ20101440. PubMed PMID: 20929442; PubMed Central PMCID: PMC2992795.

38. Guo M, Feng H, Zhang J, Wang W, Wang Y, Li Y, et al. Dissecting transcription regulatory pathways through a new bacterial one-hybrid reporter system. Genome Res. 2009;19(7):1301-8. Epub 2009/02/21. doi: 10.1101/gr.086595.108. PubMed PMID: 19228590; PubMed Central PMCID: PMC2704442.

39. Morris RP, Nguyen L, Gatfield J, Visconti K, Nguyen K, Schnappinger D, et al. Ancestral antibiotic resistance in *Mycobacterium tuberculosis*. Proc Natl Acad Sci U S A. 2005;102(34):12200-5. Epub 2005/08/17. doi: 10.1073/pnas.0505446102. PubMed PMID: 16103351; PubMed Central PMCID: PMC1186028.

40. Rybniker J, Nowag A, van Gumpel E, Nissen N, Robinson N, Plum G, et al. Insights into the function of the WhiB-like protein of mycobacteriophage TM4--a transcriptional inhibitor of WhiB2. Mol Microbiol. 2010;77(3):642-57. Epub 2010/06/16. doi: 10.1111/j.1365-2958.2010.07235.x. PubMed PMID: 20545868.

41. Stapleton MR, Smith LJ, Hunt DM, Buxton RS, Green J. *Mycobacterium tuberculosis* WhiB1 represses transcription of the essential chaperonin GroEL2. Tuberculosis (Edinb). 2012;92(4):328-32. doi: 10.1016/j.tube.2012.03.001. PubMed PMID: 22464736; PubMed Central PMCID: PMCPMC3430963.

42. Colangeli R, Helb D, Vilcheze C, Hazbon MH, Lee CG, Safi H, et al. Transcriptional regulation of multi-drug tolerance and antibiotic-induced responses by the histone-like protein Lsr2 in *M. tuberculosis*. PLoS Pathog. 2007;3(6):e87. Epub 2007/06/26. doi: 10.1371/journal.ppat.0030087. PubMed PMID: 17590082; PubMed Central PMCID: PMC1894825.

43. Dame RT. The role of nucleoid-associated proteins in the organization and compaction of bacterial chromatin. Molecular microbiology. 2005;56(4):858-70. doi: 10.1111/j.1365-2958.2005.04598.x. PubMed PMID: 15853876.

44. Ma S, Minch KJ, Rustad TR, Hobbs S, Zhou SL, Sherman DR, et al. Integrated Modeling of Gene Regulatory and Metabolic Networks in *Mycobacterium tuberculosis.* PLoS Comput Biol. 2015;11(11):e1004543. doi: 10.1371/journal.pcbi.1004543. PubMed PMID: 26618656; PubMed Central PMCID: PMCPMC4664399.

45. Bhaskar A, Chawla M, Mehta M, Parikh P, Chandra P, Bhave D, et al. Reengineering redox sensitive GFP to measure mycothiol redox potential of *Mycobacterium tuberculosis* during infection. PLoS Pathog. 2014;10(1):e1003902.

Epub 2014/02/06. doi: 10.1371/journal.ppat.1003902. PubMed PMID: 24497832; PubMed Central PMCID: PMC3907381.

46. Buchmeier NA, Newton GL, Koledin T, Fahey RC. Association of mycothiol with protection of *Mycobacterium tuberculosis* from toxic oxidants and antibiotics. Mol Microbiol. 2003;47(6):1723-32. Epub 2003/03/08. PubMed PMID: 12622824.

47. Singh A, Mai D, Kumar A, Steyn AJ. Dissecting virulence pathways of *Mycobacterium tuberculosis* through protein-protein association. Proc Natl Acad Sci U S A. 2006;103(30):11346-51. PubMed PMID: 16844784.

48. Feng L, Chen Z, Wang Z, Hu Y, Chen S. Genome-wide characterization of monomeric transcriptional regulators in *Mycobacterium tuberculosis*. Microbiology. 2016;162(5):889-97. doi: 10.1099/mic.0.000257. PubMed PMID: 26887897.

49. Vaubourgeix J, Lin G, Dhar N, Chenouard N, Jiang X, Botella H, et al. Stressed Mycobacteria Use the Chaperone ClpB to Sequester Irreversibly Oxidized Proteins Asymmetrically Within and Between Cells. Cell Host Microbe. 2015;17(2):178-90. Epub 2015/01/27. doi: 10.1016/j.chom.2014.12.008. PubMed PMID: 25620549.

50. Fay A, Glickman MS. An essential nonredundant role for mycobacterial DnaK in native protein folding. PLoS Genet. 2014;10(7):e1004516. doi: 10.1371/journal.pgen.1004516. PubMed PMID: 25058675; PubMed Central PMCID: PMCPMC4109909.

51. Burian J, Ramon-Garcia S, Howes CG, Thompson CJ. WhiB7, a transcriptional activator that coordinates physiology with intrinsic drug resistance in *Mycobacterium tuberculosis*. Expert Rev Anti Infect Ther. 2012;10(9):1037-47. Epub 2012/10/31. doi: 10.1586/eri.12.90. PubMed PMID: 23106278.

52. Facey PD, Hitchings MD, Saavedra-Garcia P, Fernandez-Martinez L, Dyson PJ, Del Sol R. *Streptomyces coelicolor* Dps-like proteins: differential dual roles in response to stress during vegetative growth and in nucleoid condensation during reproductive cell division. Molecular microbiology. 2009;73(6):1186-202. doi: 10.1111/j.1365-2958.2009.06848.x. PubMed PMID: 19719512.

53. Ouafa ZA, Reverchon S, Lautier T, Muskhelishvili G, Nasser W. The nucleoid-associated proteins H-NS and FIS modulate the DNA supercoiling response of the pel genes, the major virulence factors in the plant pathogen bacterium *Dickeya dadantii*. Nucleic acids research. 2012;40(10):4306-19. doi: 10.1093/nar/gks014. PubMed PMID: 22275524; PubMed Central PMCID: PMCPMC3378864.

54. Ushijima Y, Ohniwa RL, Maruyama A, Saito S, Tanaka Y, Morikawa K. Nucleoid compaction by MrgA(Asp56Ala/Glu60Ala) does not contribute to staphylococcal cell survival against oxidative stress and phagocytic killing by macrophages. FEMS microbiology letters. 2014;360(2):144-51. doi: 10.1111/1574-6968.12598. PubMed PMID: 25227518.

55. Bartek IL, Woolhiser LK, Baughn AD, Basaraba RJ, Jacobs WR, Jr., Lenaerts AJ, et al. *Mycobacterium tuberculosis* Lsr2 is a global transcriptional regulator required for adaptation to changing oxygen levels and virulence. mBio. 2014;5(3):e01106-14. doi: 10.1128/mBio.01106-14. PubMed PMID: 24895305; PubMed Central PMCID: PMCPMC4049101.

56. Dwyer DJ, Camacho DM, Kohanski MA, Callura JM, Collins JJ. Antibiotic-induced bacterial cell death exhibits physiological and biochemical hallmarks of apoptosis. Molecular cell. 2012;46(5):561-72. doi: 10.1016/j.molcel.2012.04.027. PubMed PMID: 22633370; PubMed Central PMCID: PMCPMC3710583.

57. Flardh K, Findlay KC, Chater KF. Association of early sporulation genes with suggested developmental decision points in *Streptomyces coelicolor* A3(2). Microbiology. 1999;145 (Pt 9):2229-43. doi: 10.1099/00221287-145-9-2229. PubMed PMID: 10517576.

58. Wu ML, Gengenbacher M, Dick T. Mild Nutrient Starvation Triggers the Development of a Small-Cell Survival Morphotype in Mycobacteria. Front Microbiol. 2016;7:947. doi: 10.3389/fmicb.2016.00947. PubMed PMID: 27379076; PubMed Central PMCID: PMCPMC4909757.

59. Rustad TR, Harrell MI, Liao R, Sherman DR. The enduring hypoxic response of *Mycobacterium tuberculosis.* PLoS One. 2008;3(1):e1502. PubMed PMID: 18231589.

60. Betts JC, Lukey PT, Robb LC, McAdam RA, Duncan K. Evaluation of a nutrient starvation model of *Mycobacterium tuberculosis* persistence by gene and protein expression profiling. Mol Microbiol. 2002;43(3):717-31. PubMed PMID: 11929527.

61. Venkataraman B, Vasudevan M, Gupta A. A new microarray platform for whole-genome expression profiling of *Mycobacterium tuberculosis*. J Microbiol Methods. 2014;97:34-43. Epub 2013/12/25. doi: 10.1016/j.mimet.2013.12.009. PubMed PMID: 24365110.

Supporting Information

S1 Fig. Generation of *MtbΔwhiB4*.

S2 Fig. Functional annotation of genes affected by CHP stress in wt *Mtb and MtbΔwhiB4*.

S3 Fig. DNA bindings assays using oxidized apo-WhiB4.

S4 Fig. *In vivo* thiol-trapping to study redox state of WhiB4 under CHP stress.

S5 Fig. Apo-WhiB4 protects DNA from DNase I and Fenton damage.

S6 Fig. WhiB4 over-expression condenses DNA in *Msm*, but not in *E. coli.*

S7 Fig. Survival of wt *Mtb* under different CHP concentrations.

S8 Fig. Confocal microscopic images of wt *Mtb* cells after prolonged oxidative stress.

S9 Fig. DNA damage analysis by Quantitative-PCR.

S10 Fig. Nucleoid condensation state of *MtbΔmshA* and *mshA-comp*.

S11 Fig. Stress phenotypes of wt *Mtb*, *MtbΔwhiB4* and *whiB4-OE* strains *in vitro*.

S12 Fig. WhiB4 dependent regulation of intramycobacterial E_{MSH} inside immune-activated macrophages.

S1 Table (raw excel file). Differentially regulated genes in microarray in wt *Mtb* and *MtbΔwhiB4* in response to CHP [(log values) 2-fold up- and down- regulation, $p \leq 0.05$].

S2 Table. qRT-PCR analysis of CHP responsive genes.

S3 Table (raw excel file). Nodes and edges representing oxidative stress network in wt *Mtb* and *MtbΔwhiB4*.

S4 Table. Network properties under different conditions.

S5 Table. Sequences of oligonucleotides used in this study.

Note S1. Protein-protein interaction network reconstruction and analysis.

Note S2. Network subtraction approach to identify WhiB4-specific netwroks under CHP stress conditions.

SI Materials and Methods. Miscellaneous methodologies used in the study.

Supporting Information

Redox-dependent condensation of mycobacterial genome by WhiB4

Manbeena Chawla[1], Mansi Mehta[1#], Pankti Parikh[1#], Saurabh Mishra[1], Prashant Shukla[1,2], Priyanka Baloni[3], Manika Vij [4,5], H N Verma [6], Munia Ganguli [4,5], Nagasuma Chandra[3], and Amit Singh[1*]

[1] Department of Microbiology and Cell Biology, Centre for Infectious Disease Research, Indian Institute of Science, Bangalore 560012, India, [2] Immunology group, International Centre for Genetic Engineering and Biotechnology, New Delhi 110067, India, [3] Department of Biochemistry, Indian Institute of Science, Bangalore 560012, India, [4] Department of Structural Biology, CSIR-Institute of Genomics and Integrative Biology, South Campus, Mathura Road, New Delhi 110020, India, [5] Academy of Scientific and Innovative Research (AcSIR), Anusandhan Bhawan, 2 Rafi Marg, New Delhi 110001, India, [6] Jaipur National University, Jagatpura, Jaipur 302017, India.

# Authors contributed equally to this work.

SI Figures

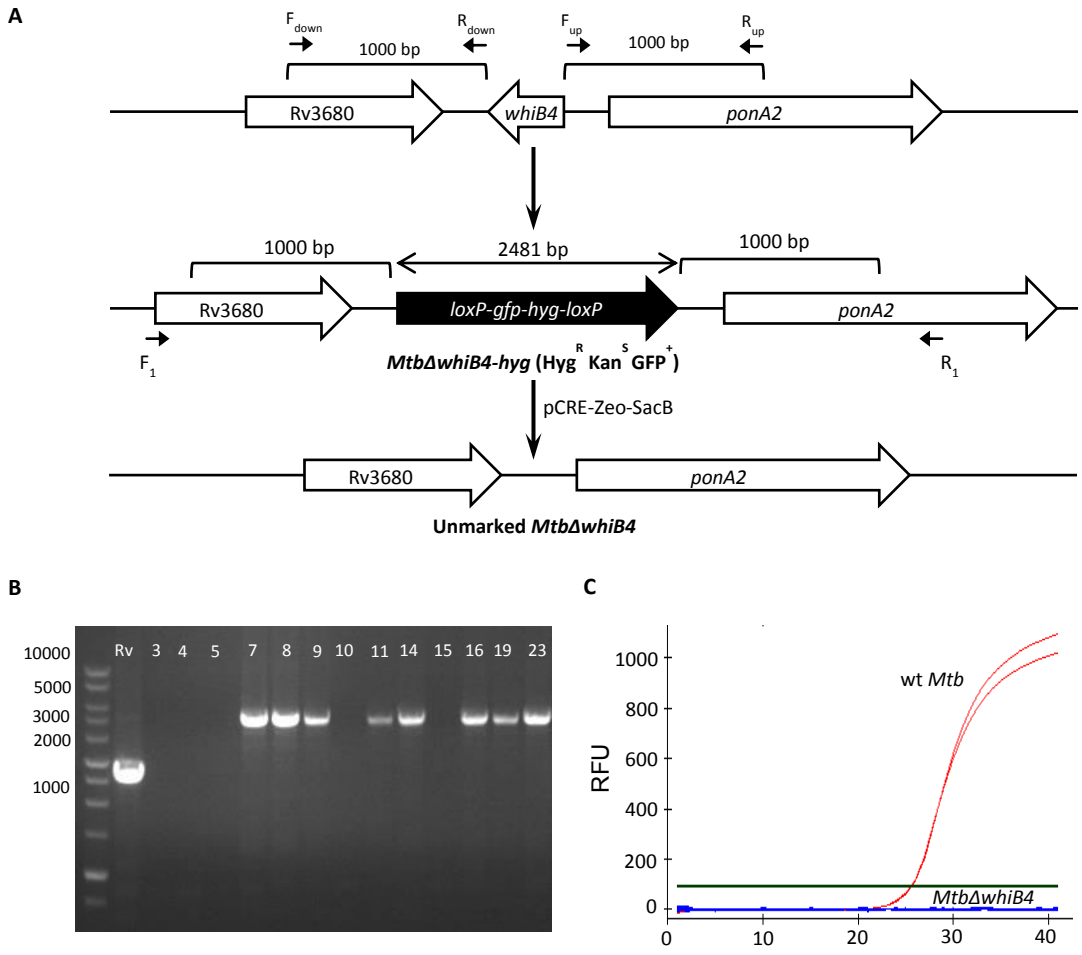

Fig. S1: (A) A step-wise illustration for construction of unmarked strain of *MtbΔwhiB4*. Upper panel denotes wt *Mtb whiB4* loci. After allelic exchange, entire *whiB4* ORF in *Mtb* genome was replaced by right and left flanking regions of *whiB4* along with loxP-*hyg*-*gfp*-loxP cassette. This knock out strain was unmarked by expressing Cre recombinase to remove *hyg*-*gfp* cassette. **(B)** Genomic DNA was isolated from putative *MtbΔwhiB4* colonies (7, 8, 9, 11, 14, 16, 19 and 23) which were $Kan^{S}Hyg^{R}GFP^{+}$ and replacement of *whiB4* allele with Hyg/GFP cassette was confirmed using PCR with F1 and R1 primers (S5 Table). An increase in amplicon size from 1.2 kb to 3.3 kb due to insertion of loxP-*hyg*-*gfp*-loxP cassette was observed in case of mutant clones, confirming the double crossover event. **(C)** RNA

was isolated from logarithmically grown wt *Mtb* and the putative *MtbΔwhiB4* clones. qRT-PCR for *whiB4* was done using *whiB4* specific oligonucleotides (S5 Table) and C_t values were plotted to assess the expression.

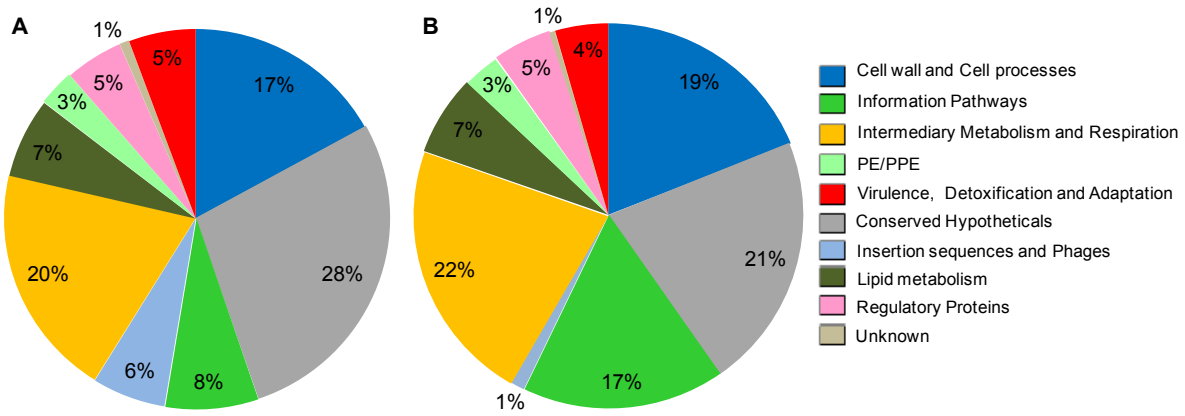

Fig. S2: Pie chart represents the relative fraction of various pathways affected by CHP stress in wt *Mtb and MtbΔwhiB4*. Genes were classified in 10 classes based on the annotation given in TubercuList database.

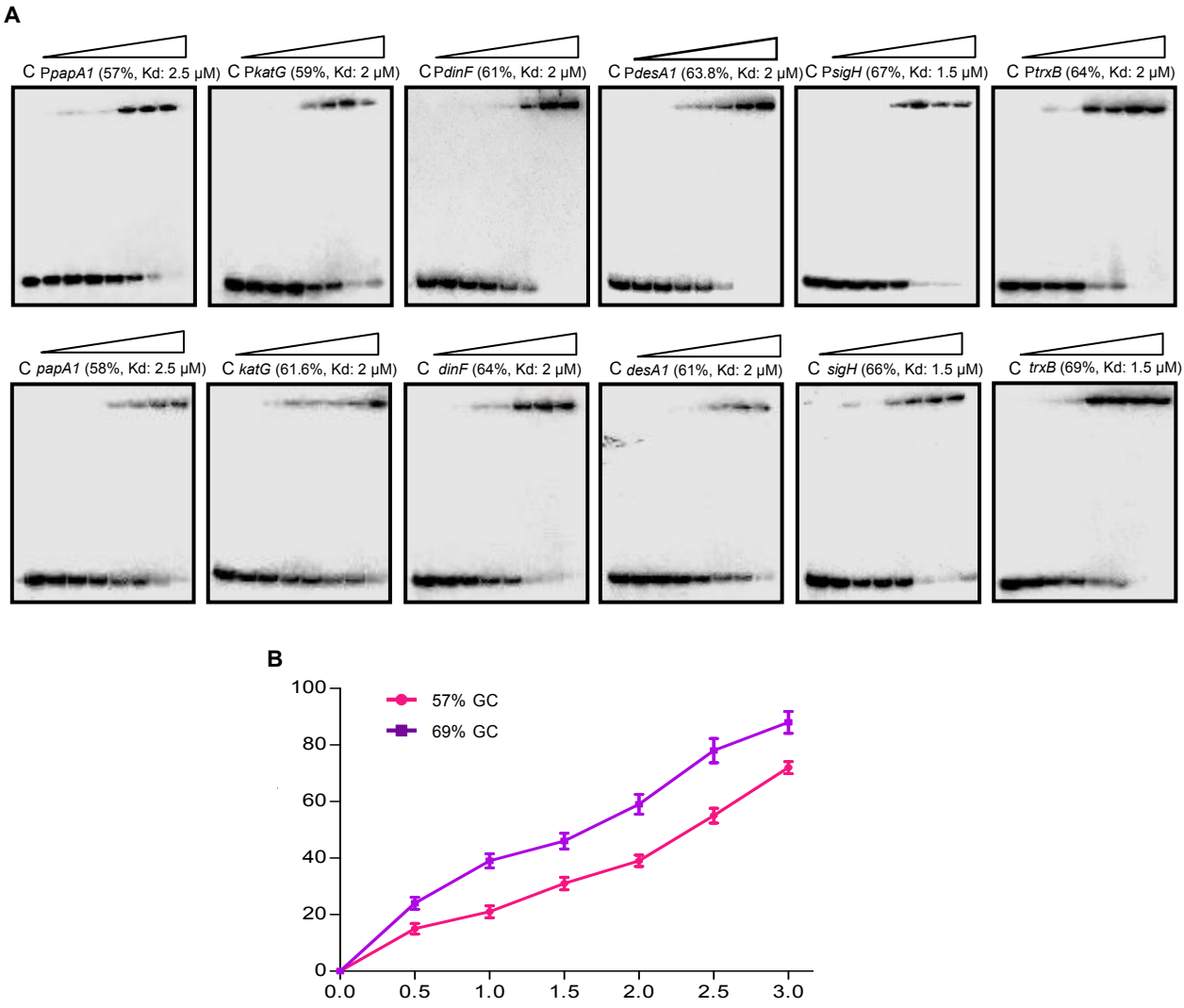

Fig. S3: WhiB4 binds to both the intragenic and intergenic regions of *Mtb* genes. **(A)** EMSAs were performed with 0.2 nM of ɣ-^{32}P labeled promoter DNA fragments (upper panel) and intragenic DNA fragments (lower panel) of genes regulated by WhiB4 as per the expression data. The concentrations of oxidized apo-WhiB4 used were ranging from 0.5 to 3.5 μM. C: DNA binding in the absence of WhiB4 in each panel. **(B)** Graph depicting the relation between the fractions of bound radioactively labeled DNA probe with highest and lowest GC % and the concentration of apo-WhiB4 in the binding reaction. Standard deviations (SD) were less than 10% of the mean values.

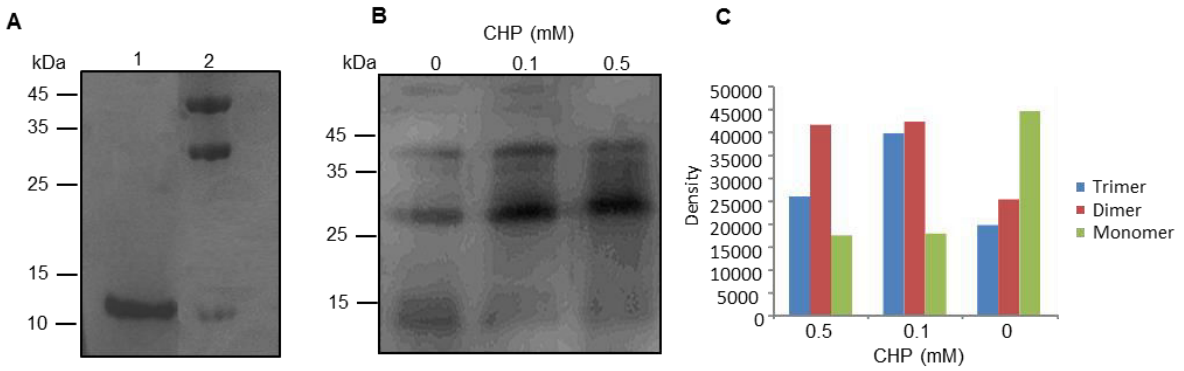

Fig. S4: **Formation of disulfide-linked oligomers of WhiB4 *in vivo*. (A)** 3 µg of aerobically purified histidine-tagged apo-WhiB4 was either (Lane 1) reduced by 500 mM β-ME or (Lane 2) oxidized by 30 mM Diamide and resolved on a 12% non-reducing SDS-PAGE. Apo-WhiB4 bands were visualised by silver staining. **(B)** *MtbΔwhiB4* strain expressing histidine-tagged WhiB4 from its native promoter was used. Using qRT-PCR, we verified that the expression of *his-whiB4* transcript from its native promoter was comparable to the expression of endogenous *whiB4* transcript in *wt Mtb*. To minimize the possibility of O_2-induced thiol oxidation and subsequent oligomerization of apo-WhiB4 during cell-free extract preparation, cells were pretreated with the thiol-alkylating agent NEM as described [9]. Approximately 25 µg of cell-free extract was resolved on a 12% non-reducing SDS-PAGE and immuno-blotted using anti-his. **(C)** Measurement of band-intensity cleary indicates a significant increase in WhiB4 dimer and trimer relative to monomer upon CHP stress

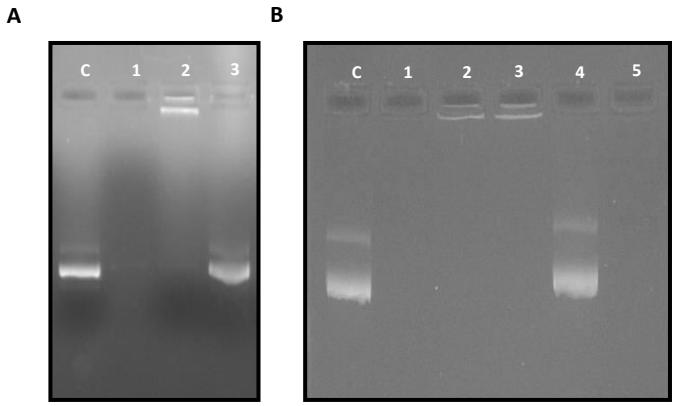

Fig. S5: Apo-WhiB4 protects DNA from DNase I and Fenton damage. **(A)** Lane 1: Plasmid DNA treated with 1 unit of DNase I. Lane 2: Plasmid DNA in complex with apo-WhiB4. Lane 3: Plasmid DNA-apo-WhiB4 complex was treated with 1 unit of DNase I. Sample was treated with 6% SDS and 4 mg/ml protease K for 30 minutes at 37^{o}C before analysis on a 1% agarose gel. **(B)** Plasmid DNA was treated with 100 µM $FeSO_4$ and 10 mM H_2O_2 (lane 1). Plasmid DNA was incubated with apo-WhiB4

(lane 2) and then treated with 100 µM $FeSO_4$ and 10 mM H_2O_2 (lane 3). As a control, DNA was incubated with BSA (lane 4) and then exposed to the Fenton reaction (lane 5). Samples were analyzed on a 1% agarose gel. C: Plasmid DNA alone.

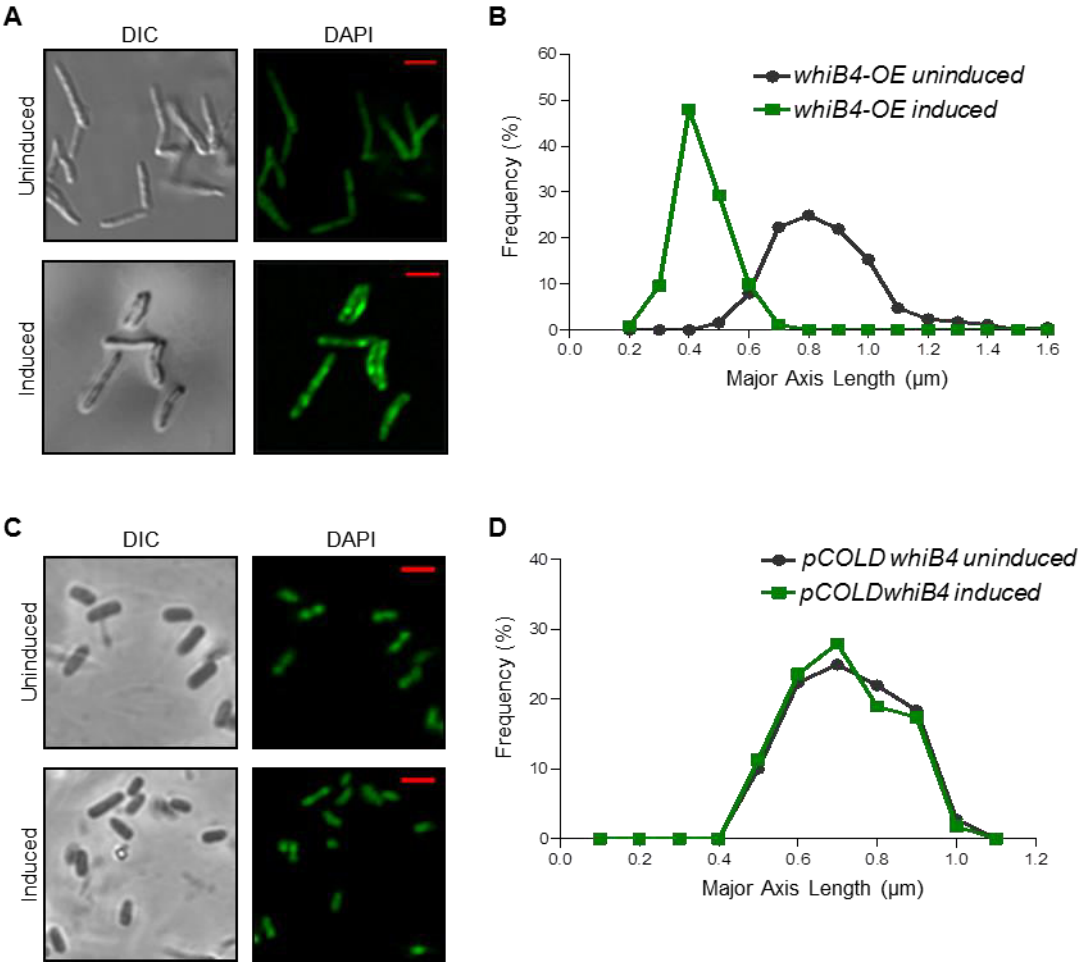

Fig. S6: WhiB4 over-expression condenses DNA in *Msm*, but not in *E. coli*. WhiB4 was over-expressed in *Msm* **(A)** and in *E. coli* **(C)** and nucleoids were stained with DAPI (pseudo colored green) and visualized by confocal microscopy (63X). **(B and D)** Histogram showing distribution of the major axis length of the nucleoids (n=200). The histogram was generated by plotting the percentage of nucleoids per 0.1 µm size intervals with respect to the major axis length of each nucleoid. The scale of images is 1 µm. Induction of WhiB4 in cold conditions from pCOLD vector resulted in ~ 80% of protein in the soluble fraction ruling out the possibility that the lack of genome condensation is due to insolublity of WhiB4 in *E.coli*.

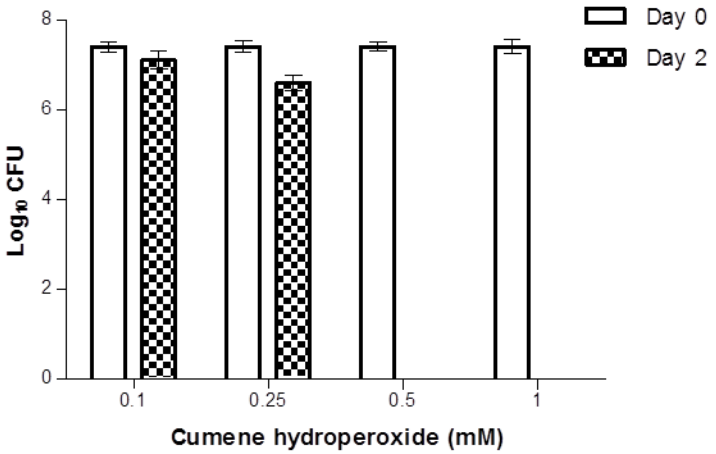

Fig. S7: Survival of wt *Mtb* under oxidative stress. Survival of wt *Mtb* treated with 0.1, 0.25, 0.5 and 1 mM CHP for 2 days at 37^{o}C was measured by CFUs. Data shown is the average of experiments performed in triplicates. Error bars represent SD from the mean.

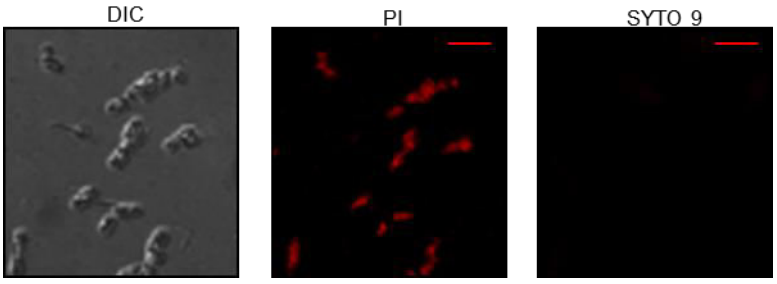

Fig. S8: Confocal microscopic images (63X) of wt *Mtb* cells after prolonged oxidative stress. wt *Mtb* was exposed to 0.5 mM CHP treatment for 48 h and cells were stained with SYTO9 and Propidium iodide (Pi) combination. Red fluorescence emitted by Pi stained cells indicate cell death. The scale of images is 1µm.

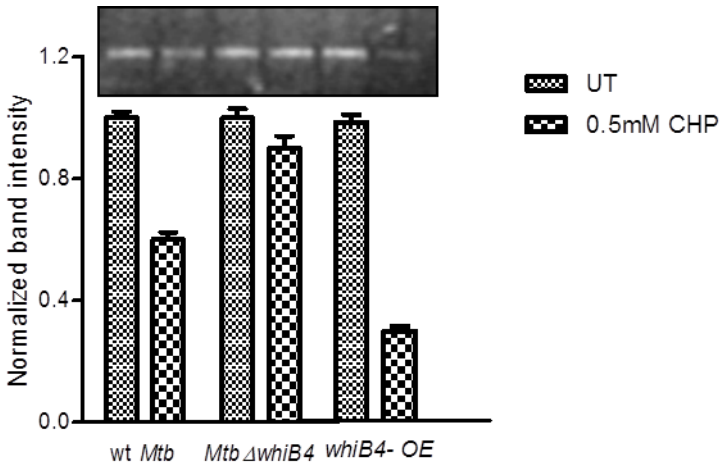

Fig. S9: DNA damage analysis by Quantitative-PCR. PCR amplification of a 10kb fragment using genomic DNA (of wt *Mtb, MtbΔwhiB4* and *whiB4-OE* strains) treated with 0.5 mM CHP for 24 h. The amplification signal for untreated and treated conditions was normalized and the densitometric analysis was plotted. Data shown is the average of experiments performed in triplicates. Error bars represent SD from the mean.

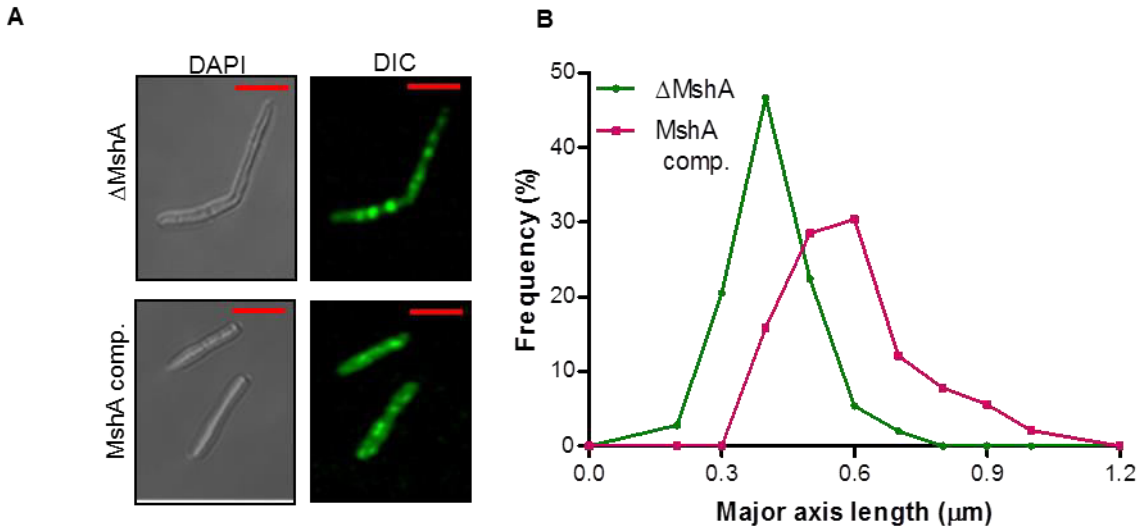

Fig. S10: (A) Nucleoids of *MtbΔmshA* and *mshA-comp* strains were stained with DAPI (pseudo colored green) and visualized under confocal microscope (63X). **(B)** Histogram showing distribution of the major axis length of the nucleoids (n=200) in the two strains. The histogram was generated by plotting the percentage of

nucleoids per 0.1 µm size intervals with respect to the major axis length of each nucleoid. The scale of images is 3 µm.

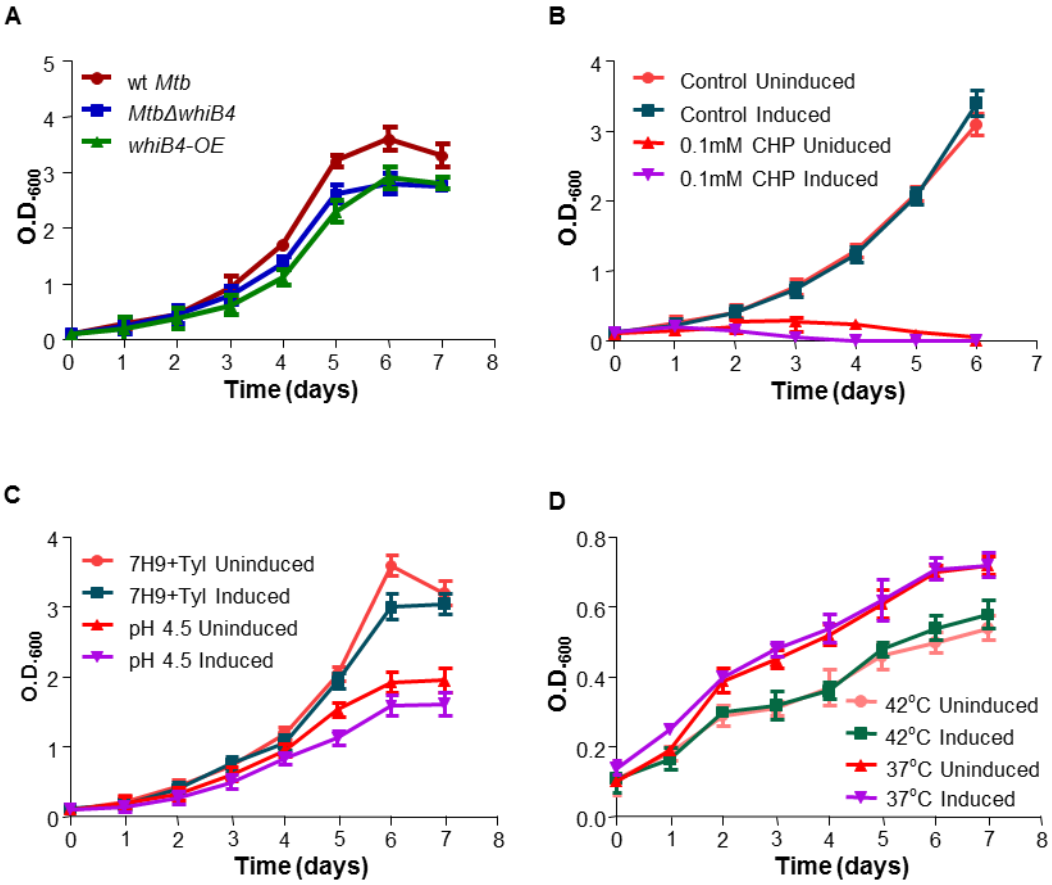

Fig. S11: (A) Aerobic growth phenotype of wt *Mtb*, *MtbΔwhiB4* and *whiB4-OE* strains was determined by growing cells in 7H9 medium. The *whiB4-OE* strain (induced and uninduced) was exposed to different stress conditions, **(B)** 0.1 mM CHP, **(C)** pH 4.5, **(D)** 42ºC. Growth was monitored at different time intervals by measuring absorbance at 600 nm. Data shown is the average of two experiments performed in triplicates. Error bars represent SD from the mean.

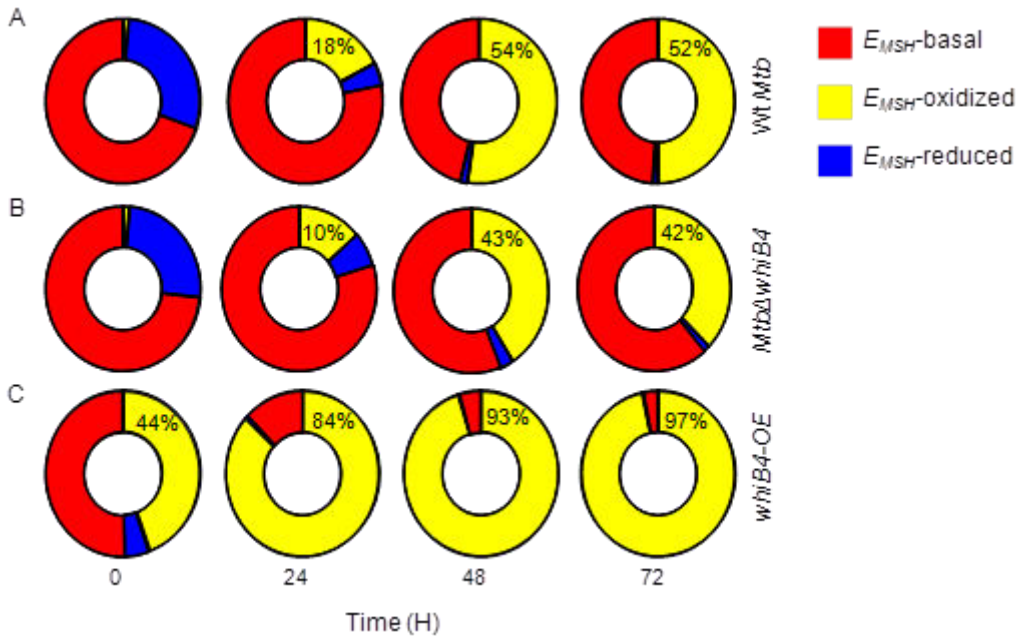

Fig.S12: WhiB4 dependent regulation of intramycobacterial E_{MSH} inside macrophages. Activated RAW 264.7 macrophages were infected with Mrx1-roGFP2 expressing **(A)** wt *Mtb*, **(B)** *MtbΔwhiB4*, and **(C)** *whiB4-OE* strains at a moi of 10. At indicated time points, ~ 30,000 infected macrophages were analyzed by flow cytometry, intramycobacterial E_{MSH} was measured, and percentage of bacilli in each subpopulation was determined. Consistent with our previous findings, macrophage environment induced heterogeneity in the E_{MSH} of *Mtb* cells, which can be segregated into three subpopulations *i.e.* E_{MSH}-oxidized, E_{MSH}-basal and E_{MSH}-reduced [10]. The percentage of bacilli in each subpopulation was plotted as a pie chart as described earlier [10]. The "0" h time point refers to time immediately after infection with *Mtb* strains for 4h.

Table S1: Differentially regulated genes in microarray in wt *Mtb* and *MtbΔwhiB4* in response to CHP [(log values) 2-fold up- and down- regulation, $p \leq 0.05$]. (Enclosed as a separate excel spread sheet).

Table S2: qRT-PCR analysis of CHP responsive genes.

Genes	Fold change (*MtbΔwhiB4*/ *wt Mtb*)	Fold change (CHP treated wt *Mtb*/wt *Mtb*)	Fold change (CHP treated *MtbΔwhiB4*/ *MtbΔwhiB4*)	Fold change (CHP treated *MtbΔwhiB4*/ CHP treated wt *Mtb*)	Fold change (*whiB4-OE*/ *MtbΔwhiB4*)	Fold change (CHP treated *whiB4-OE*/ CHP treated *MtbΔwhiB4*)
ahpC	2.65 ±0.47	12.39 ±0.65	1.85 ±0.30	1.14 ±0.29	-3.85 ±0.49	-10.67 ±1.52
ahpD	2.84 ±0.56	3.31 ±0.61	1.39 ±0.23	1.30 ±0.18	-6.66 ±0.46	-9.24 ±0.29
trxB2	-1.30 ±0.11	5.70 ±0.91	11.96 ±1.29	1.65 ±0.29	-2.22 ±0.34	2.04 ±0.19
trxC	1.50 ±0.50	3.49 ±0.60	11.60 ±0.67	3.23 ±0.31	-3.90 ±0.43	1.61 ±0.34
katG	3.13 ±0.64	29.51 ±3.61	15.98 ±1.57	3.95 ±0.37	-1.57 ±0.31	-5.93 ±0.76
recA	1.18 ±0.17	22.32 ±2.06	16.41 ±1.80	-1.27 ±0.24	-1.65 ±0.37	-2.77 ±0.67
sigB	1.52 ±0.36	5.24 ±0.03	11.55 ±1.97	2.90 ±0.71	-1.31 ±0.16	-1.32 ±0.28
sigH	2.15 ±0.35	3.31 ±0.77	15.09 ±0.53	8.78 ±0.54	2.51 ±0.24	1.67 ±0.22
hsp	4.01 ±1.18	41.75 ±2.73	56.89 ±2.49	4.33 ±0.28	-6.69 ±0.60	-1.37 ±0.24
furA	6.63 ±0.73	11.31 ±1.73	16.16 ±1.04	7.55 ±0.35	-1.79 ±0.40	-6.49 ±0.49
ppsC	3.36 ±0.81	1.26 ±0.35	1.19 ±0.12	1.84 ±0.77	1.43 ±0.16	-1.12 ±0.05
lsr2	1.38 ±0.13	-1.30 ±0.14	1.76 ±0.06	3.14 ±0.19	-3.76 ±0.63	-6.20 ±0.55
gyrB	2.19 ±0.22	1.56 ±0.15	-1.51 ±0.09	-1.07 ±0.06	-3.90 ±0.22	-4.50 ±0.24
gyrA	1.14 ±0.08	-1.15 ±0.09	-1.14 ±0.01	1.19 ±0.14	-1.94 ±0.15	-4.49 ±0.37
topA	1.19 ±0.08	-3.34 ±0.34	-4.56 ±0.45	-1.18 ±0.15	-1.98 ±0.14	-2.61 ±0.34
mmr	2.22 ±0.44	1.91 ±0.29	4.23 ±0.56	4.50 ±0.18	-2.39 ±0.42	-2.86 ±0.38
pks3	2.02 ±0.68	-1.34 ±0.10	-1.57 ±0.22	4.63 ±0.55	-3.54 ±0.77	-6.51 ±0.90
papA1	1.58 ±0.35	1.32 ±0.17	1.72 ±0.20	2.30 ±0.21	-2.65 ±0.51	-7.98 ±0.32
ponA1	1.47 ±0.34	-1.30 ±0.06	-1.63 ±0.33	1.43 ±0.22	-1.69 ±0.49	-2.57 ±0.57
pbpA	1.31 ±0.23	-1.70 ±0.29	-1.41 ±0.26	1.18 ±0.16	-1.41 ±0.36	-1.42 ±0.22

**sseA*	-1.25±0.12	1.103±0.019	-1.8±0.023	-0.89±0.017	-1.1±0.23	-0.69±0.13
**GroEL*	1.28±0.034	1.14±0.014	-1.28±0.065	-1.08±0.02	-1.08±0.5	-1.13±0.5
**trxA*	-1.61±0.12	-1.356±0.034	-1.18±0.035	-1.255±0.03	-1.15±0.03	-1.04±0.1
**papA3*	1.17±0.32	-1.1±0.011	-1.42±0.05	-1.06±0.072	-1.23±0.31	-1.1±0.08
**dnaK*	1.29±0.3	2.21±0.09	-1.24±0.21	-1.52±0.12	-1.85±0.17	-1.01±0.3
alkA	1.05±0.03	-2.03±0.32	-1.72±0.4	1.98±0.63	-1.02±0.2	-6.3±0.84
mutM1	1.18±0.09	-3.62±0.87	-2.27±0.34	1.93±0.57	1.07±0.21	-5.6±0.47
mutY	1.08±0.1	-2.3±0.42	-1.08±0.12	1.51±0.13	-1.26±0.08	-4.9±0.74
ung	1.37±0.3	-2.26±0.08	-1.37±0.22	1.54±0.43	0.12±0.09	-9.13±0.66

*genes exhibiting comparable levels of expression in wt *Mtb, MtbΔwhiB4, and WhiB4-OE strains.*

Table S3. Nodes and edges representing oxidative stress network in wt *Mtb* and *MtbΔwhiB4* (Enclosed as a separate excel spread sheet).

.

Table S4: Network properties under various comparisons.

	MtbΔwhiB4 vs. wt *Mtb*	wt *Mtb* CHP vs. wt *Mtb*	*MtbΔwhiB4* CHP vs. *MtbΔwhiB4*	*MtbΔwhiB4* CHP vs. wt *Mtb* CHP
No. of genes down-regulated (≥ 2-fold, p≤ 0.05)	94	269	348	48
No. of genes up-regulated (≥ 2-fold, p≤0.05)	91	345	81	84

No. of Paths with Path Length ≥ 3	9152652	9155498	9161930	9166624
Paths score cut-off	0.03	0.01	0.3	0.1
No. of Paths with the Path Score cut-off	7591	12754	10953	4497
% of paths considered for sub-network analysis	0.08	0.14	0.12	0.05
No. of Nodes in the sub-network	309	259	264	216
No. of Interactions in the sub-network	397	335	330	288

The number of nodes and the interactions varied in each condition based upon the threshold selected for path-score.

Table S5: Sequences of primers used in this study

Gene Name	Primer Sequence (for qRT-PCR)
ahpC	F: 5' TTTGGCCGAAAGACTTCACG 3' R: 5' GACATCAAGCGCGAACTCAG 3'
ahpD	F: 5' CGAAATCCGCAGGTATTAGC 3' R: 5' CATACCGAAAGCCAACTTCG 3'
whiB4	F: 5' GGATCAGCTCGTGTCAGGAA 3' R: 5' AGTGGCTATCCGGCGGTGCC 3'

16s rRNA	F: 5' TTGACGGTAGGTGGAGAAGA 3' R: 5' CGCAAGGCTAAAACTCAAAGG 3'
pks3	F: 5' GATTCACCGGCACCAGTAAC 3' R: 5' GCAAGAGCGAGATCGCTTTC 3'
trxB2	F: 5' ATGACCGCCCCGCCTGTCCA 3' R: 5' CGGCGCCAGCTGGGCACGGG 3'
trxC	F: 5'ATGACCGATTCCGAGAAGTC 3' R: 5'GCAAGGTCCACACCATGTCG 3'
katG	F: 5'GTGCCCGAGCAACACCCACC 3' R: 5'GGGCCACCAGTCCTGGTTTC 3'
recA	F: 5'ATGACGCAGACCCCCGATCG 3' R: 5'GACCGAAATCGGCTGACGCG 3'
sigB	F: 5'AGCCCCGCGGCGGACCTCGT 3' R: 5'ATGCTCGGCATACAACCCGG 3'
sigH	F: 5'ACAGACGAGGAGTTGACCGC 3' R: 5'CTCCTGGAGCAAGTCCTCGG 3'
hsp	F: 5'CTACGTGACTTCTTCGGCCC 3' R: 5'CAGTTCCAAACGGACCACCG 3'
ppsC	F: 5'AGTTGTTGGAACAACTTTCG 3' R: 5'TCCAGGCGCGCCGTGAGATC 3'
lsr2	F:5'GACCGGGGAGTCTATCCGTA 3'

	R:5'CGACCGTTTCGTCGGCGGCG 3'
gyrA	F: 5'GTTCCTGGATGTCTAACGCA 3' R: 5'TCTCCTGCTCGATGTCAACC 3'
gyrB	F: 5'TGCGGCGACTCAACCGCATG 3' R: 5'CACCATTCTCGAAGGGCTGG 3'
topA	F: 5'GAGATGGAGCGTGGGCGCAG 3' R: 5'AGGCCAGCTTGCGCGCCTTG 3'
furA	F: 5'GTCATATTGTCTAGTGTGTC 3' R: 5'TGAATGCGCATCCACACGCC 3'
mmr	F: 5'ATGTACACAAAGGAGGGGTC 3' R: 5'CCACCGTGGGCCACAACCGA 3'
ponA1	F: 5'CGCTGTACCTCACCGCGGCG 3' R: 5'GGATCGTGGAGACCTGGTTG 3'
papA1	F: 5'CGCTGAAATAGGAGCTATTA 3' R: 5'ACCTGCCTCGTGCGCGAAAG 3'
pbpA	F: 5'GGTCATCGAACGCGTATGAA 3' R: 5'ACGCAGCCCGTCGGCGGTGA 3'
dnaK	F: 5'TCAGGAGGATTCACCATGGC 3' R: 5'GGTCCTGGAGCCCTCGGAGT 3'
sseA	F: 5'CCAGCGGTAGGCTCGATGAT 3' R: 5'CCGGCGCGCCCATGTGTGCC 3'

groEL	F: 5'TCCGGAGGAATCACTTCGCA 3' R: 5'CCTTGGGGCCCAATGTCACC 3'
trxA	F: 5'GGGCTGCGTTAGGGGTGCCC 3' R: 5'ACCGCTGTGCGCCCCGTGCG 3'
papA3	F: 5'GAGATCGAGCCGAGGAGGGC 3' R: 5'TCGTGTGCGCGACAGCCGAA 3'
mutM1	F: 5'ATCACTGGATGCCCGAGCTG 3' R: AGCCGTATTGAGTGTCAACC 3'
mutY	F: 5'AGTGCTTTCCACGCGGCTAC 3' R: 5'CGCTGATACCAAGCGAGAAG 3'
alkA	F: 5' TCGGTGGGCGGGTGTAATTG 3' R: 5'AAACCGCGACGACGAACCAG 3'
ung	F: 5'TGACCGTCTGTACGCGAAAG 3' R: 5'ATCTCGGCCCGCAAGAACTG 3'

Primer Name	**Primer Sequence (used for ChIP qPCR analysis)**
P*trxC*	F: 5'GAAACCACCCTGCCGGTAAC 3' R: 5'TAACCGCCTGGCGATAGGTG 3'
P*gyrB*	F: 5'AGAGCCTCGAGGACGAAGCG 3' R: 5'ACCTGCGACTACCGGCTGTT 3'

P*hsp*	F: 5'GAGGGGCAAATTACCGAAAA 3' R: 5'CTCGTCGGCGGACTGCGGCG 3'
P*papA3*	F: 5'ACAGTCAGGCGGTTGGTATC 3' R: 5'GCGAACCGTGGTGATCTTTG 3'
P*trxA*	F: 5'GGGTGACCATACGGGACGAA 3' R: GCGCAACTGCCTTCGGTAGCA 3'
P*ahpC*	F: 5'GAGACCGGCTTCCGACCACC 3' R: 5'CCCTAGACCAACCTTAATAG 3'
P*ahpD*	F: 5'ACACCACTACCGGTTTACCC 3' R: 5'GACTTTGGCTAGCGTGACAG 3'
P*sigB*	F: 5'CCCGCCGATTGTACGTCGAA 3' R: 5' AGCTGGACATCCTGAGCCAG 3'
P*sseA*	F: 5'CCTCCGATCTGGAGGCTTAC 3' R: 5'GGCTCAAGCCGATCACATTC 3'

Primer Name	**Primer Sequence (used for EMSA analysis)**
P*desA1*	F: 5'GAATCCGAACACTCCATCCC 3' R: 5'CATGGCGCCTCCAGTTATCT 3'
P*dinF*	F: 5' AACAAGCCGAGGTCGCGGCG 3'

	R: 5’ CGGCGGCTAACCAAGCGCCG 3’
P*katG*	F: 5’ CCGGTCTTGCGGGGTTATCG 3’ R: 5’ CAACTCCTGGAAGGAATGCT 3’
P*papA1*	F: 5’ GCACTAGAGCTGCGCACTCG 3’ R: 5’ CTAATAGCTCCTATTTCAGC 3’
P*sigH*	F: 5’ TTCGGTTCCTGCAGCCACGT 3’ R: 5’ CATCTTGATTAACTGGGTCC 3’
P*trxB2*	F: 5’ TACCCGCGGACACGCCCGAC 3’ R: 5’ GGTCATGCGAGCCTTTCGAG 3’
desA	F: 5’ CGCCATGTCAGCCAAGCTGA 3’ R: 5’ GGGCTAACGACGGCTCATCG 3’
dinF	F: 5’ TTGAGCCAGGTGGGGCACCG 3’ R: 5’ CTACGCCGCGCCCGTACCG 3’
katG	F: 5’GGAATGCTGTGCCCGAGCAA 3’ R: 5’GGTTCGACGTGCGCTGATTC 3’
papA1	F: 5’TAGTGCGAATAGGACCAGTA 3’ R: 5’ACCACTAAGCTTCTCTATCT 3’
sigH	F: 5’TCAAGATGGCCGACATCGAT 3’ R: 5’CCGGGCTGCTCATGACGACA 3’
trxB2	F: 5’GGCTCGCATGACCGCCCCGC 3’ R: 5’CGTGGGAATCGGTCATCGTT 3’

Primer Name	Primer Sequence (used for cloning)
sigB	F: 5'CAATTGGCTATGGCCGATGC 3' R: 5'AAGCTTGCGGGCATACCGTC 3'
sigE	F: 5'GAATTCATACGCCGGTACGC 3' R: 5'AAGCTTTGCGGTAGCCGAAC 3'
sigH	F: 5'CAATTGCCGCAAACGAAGGG 3' R: 5'AAGCTTACACCGGGCTGCTC 3'
whiB4	F: 5'CAATTGGTGTCAGGAACCCGT 3' R: 5' AAGCTTACCGGCACCGCCGGA 3'

Primers for confirming *MtbΔwhiB4* clones.

whiB4 F_{up} - 5' ATCGAACTAGT-GATGCCGAAGTACGTTTGCGCC 3'
whiB4 R_{up} - 5' GGTCAATTTAAAT-GAGCTGATCCCTTCCTCCCGG 3'
whiB4 F_{down} - 5' GATAGTTAATTAA-CCACTCAGGGACTGCGGATAGG 3'
whiB4 R_{down} - 5' ATGCAATGCAT-CTATGGAGAAGCTGGGCCAACTG 3'
whiB4 F_1 - 5' GACGTAGTCGCAGAAGAATG 3'
whiB4 R_1 - 5' GCGAGCTACACGCGATGATG 3'

SI note 1: Protein-protein interaction network reconstruction and analysis

A weighted directed protein-protein interaction network of wt *Mtb* H37Rv was reconstructed as described in [1]. In brief, protein-protein interactions were obtained from KEGG, STRING and Reactome databases and were manually curated to infer directions. To ensure minimum false positives, interactions with confidence score greater than 700 were included in the network, unless they were experimentally verified interactions. In addition, interactions were also obtained from previously

reported gene regulatory network [2], the transcription factor- target gene interaction in *Mtb* using CHIP-seq and high-throughput experimental bacterial one-hybrid and bacterial-2-hybrid studies [3-7]. Microarray data for each condition was integrated into the network using the median intensity value as well as the fold change value as the node weights in that network.

The node weight (NW) values for each node were calculated by multiplying the normalized intensity values with the corresponding fold-change (FC) values.

$NW_i = FC_i$ x Normalized signal intensity

These node weight values were used for calculating the edge weight (EW) values. Edge-betweenness (EB) was calculated using NetworkX, a python package (https://networkx.github.io/)..

$EW = 1 / EB \times \sqrt{NW_a \times NW_B}$

The edge weight files were used as an input for calculating all vs. all shortest paths in each condition using Zen (http://www.networkdynamics.org/static/zen/html/api/algorithms/shortest_path.html). Altogether, our gene-expression weighted network consists of 3686 nodes and 34223 edges and respectively (Additional file-X) and four such networks were generated for the following conditions - *MtbΔwhiB4* vs. wt *Mtb,* wt *Mtb* CHP vs. wt *Mtb, MtbΔwhiB4* CHP vs. *MtbΔwhiB4, MtbΔwhiB4* CHP vs. wt *Mtb* CHP. Such 'condition-specific' networks efficiently capture the changes occurring in the system under various conditions such as oxidative stress and/or disruption of *whiB4*, which were then subjected to graph theory-based methods to identify the most differentially regulated paths in each condition. Visualization of the networks and calculation of

betweeness centrality for each edge was done using Cytoscape [8]. The S4 table depicts the statistics for the conditions that were analyzed.

SI note 2- Network subtraction approach to identify WhiB4-specific netwroks under CHP stress conditions.

The comparison was carried out between *MtbΔwhiB4* CHP vs. wt *Mtb* and *MtbΔwhiB4* CHP vs. wt *Mtb* CHP. The set of unique edges in *MtbΔwhiB4* CHP vs wt *Mtb* CHP in the top-scoring subnetworks were identified, as the nodes that form these edges reflect a condition-specific association.

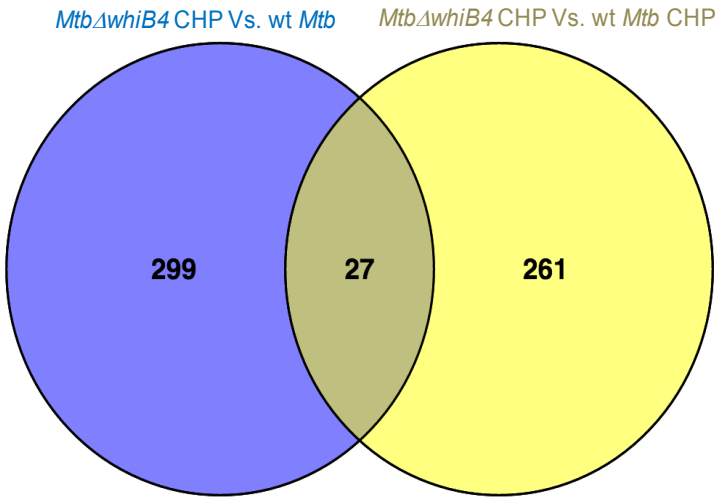

The set of 261 unique edges in *MtbΔwhiB4* CHP vs. wt *Mtb* CHP were then compared with edges in wt *Mtb* CHP vs. wt *Mtb*. This comparison gives us the information about the edges commonly present due to treatment in wt *Mtb* and *MtbΔwhiB4* and also the unique set of edges present only in *MtbΔwhiB4*.

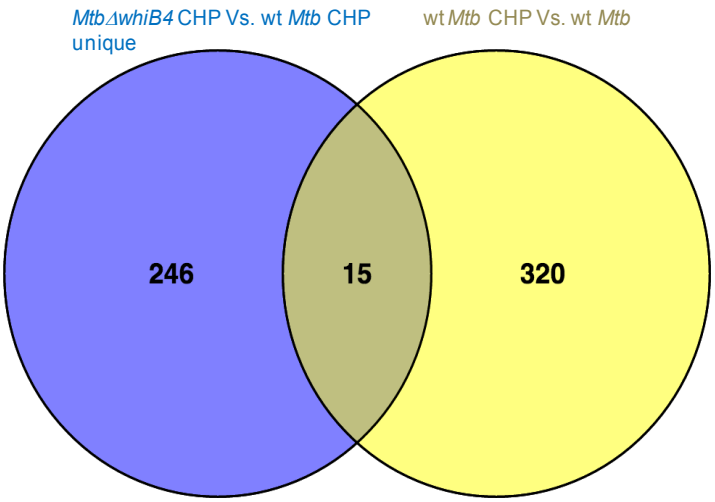

Refer to S3 and S4 tables for information of the edges common and unique to different conditions as mentioned. The fold change values are color coded and the node weight values are listed for the unique edges.

SI Materials and Methods

ChIP qPCR analysis

DNA–protein interactions were characterized by cross-linking 100 ml of culture for *MtbΔwhiB4* and *whiB4-OE* strains ($O.D._{600}$ of 0.5) with 1% formaldehyde while agitating cultures at 37^{o}C for 30 min. Crosslinking was quenched by the addition of glycine to a final concentration of 125 mM. Cells were pelleted, washed in 1 X PBS+1 X protease inhibitor cocktail (Sigma) and resuspended in IP Buffer (20 mM K-HEPES—pH 7.9, 50 mM KCl, 0.5 mM dithiothreitol and 10% glycerol) +1 X protease inhibitor cocktail. Cell debris was removed by centrifugation after lysis using Bioruptor (Diagenode) and the supernatant was used in the IP experiment. The samples were mixed with buffer IPP150 (10 mM Tris-HCl—pH 8.0, 150 mM NaCl and

0.1% NP40) and immunoprecipitation of FLAG-tagged proteins was initiated by incubating samples overnight rotating at 4 °C with (1:100 dilution) anti-FLAG antibody (Sigma) on a rotating wheel. Complexes were subsequently precipitated with Dynabeads for 3 h at 4°C. Beads were washed twice with IP buffer and once with Tris-EDTA buffer pH 7.5. Elution was performed in 50 mM Tris–HCl pH 7.5, 10 mM EDTA, 1% SDS for 40 min at 65°C. Samples were finally treated with RNAse A for 1 h at 37°C, and cross-links were reversed by incubation for 2 h at 50°C and for 8 h at 65°C in elution buffer with Protease K (Thermo Scientific). DNA was purified by phenol-chloroform extraction and quantified. The resulting ChIP-DNA was subjected to qRT PCR analysis to determine the enrichment of few promoters in the immunoprecipitated sample (*whiB4-OE*) over the control sample (*MtbΔwhiB4*).

Enrichment of the ChIP target or promoter is expressed as a fold difference between the specific antibody-immunoprecipitated sample (*whiB4-OE*) and the negative control (*MtbΔwhiB4)*. The difference between the C_t values (ΔC_t) for each target is calculated by C_t (elute) − C_t (input). Next, the $\Delta\Delta C_t$ values [ΔC_t (experimental sample) − ΔC_t (control)] are calculated for all targets. The fold difference between the experimental sample and the control is calculated by using $2^{(-\Delta\Delta Ct)}$.

qRT-PCR

Total RNA was isolated from logarithmically grown cells of wt *Mtb*, *MtbΔwhiB4 and whiB4-OE* strains and qRT-PCR was performed using gene specific primers (Table S5) as described [9].

***In vivo* thiol-trapping analysis**

Histidine-tagged WhiB4 was expressed under its native promoter in *MtbΔwhiB4*. At an O.D.$_{600}$ of 0.4, *MtbΔwhiB4* expressing histidine-tagged WhiB4 was treated with 0.1 and 0.5 mM CHP for 24 h. Cultures were treated with 10 mM NEM for 5 min to block the thiol-state of WhiB4. Bacterial pellets were resuspended in lysis buffer [300 mM NaCl, 20 mM Na-Phosphate, 10% Glycerol and 1X protease inhibitor (Amresco Inc.), pH 7.5] and lysed using bead beater (MP Biomedicals). Approximately 30 µg of total cell lysate was resolved by 12% non-reducing SDS-PAGE. Proteins were transferred on to 0.2 µm PVDF membrane and used for Western blot. Western blot analysis was achieved using 1:20,000 dilution of anti-His antibody (GE Life Sciences) for 12 h. The blotted membrane was developed with a 1:20,000 dilution of peroxidase-conjugated anti-mouse IgG (Cell Signaling) and an enhanced chemiluminescence substrate (GE Amersham).

The apo-form of aerobically purified WhiB4 was either exposed to 30mM diamide (Sigma) or 500mM β-Me and resolved by 12% non-reducing SDS-PAGE. Proteins were visualised by silver staining the gel.

Immuno-blot analysis

The expression of WhiB4 in the *whiB4-OE* and *whiB4-cys3-OE* strains was induced by 200 ng/ml ATc. For immuno-blot assay, bacterial cells were processed as described earlier. WhiB4 was detected using anti-FLAG primary antibody. The blot was developed with enhanced chemiluminescence (ECL, Bio-Rad).

Confocal microscopy

Various *Mtb* and *Msm* strains were grown to exponential phase (O.D.$_{600}$ of 0.3) in 7H9 medium and WhiB4 expression was induced as described [9]. The *E. coli*

strain harbouring pCOLD-WhiB4 was grown aerobically till $O.D._{600}$ of 0.5 and expression was induced by 0.5 mM IPTG at 16^{o}C for 24h. Cell were fixed with paraformaldehyde (PFA) and washed with 1X PBS and stained with 4',6-diamino-2-phenylindole (DAPI, 1 µg/ml, Invitrogen). The bacterial cells were visualized for DAPI fluorescence (excitation at 350 nm and emission at 470 nm) in a Leica TCS Sp5 confocal microscope under a 63X oil immersion objective. Quantification of nucleiod size (major axis) of more than 200 cells was carried out using ZenLite imaging software (Zeiss 710).

Immunofluorescence microscopy

The *whiB4-OE* strain was fixed with 4% PFA, washed with 1X PBS and permeabilized using 0.1% of Triton-X 100. Cells were blocked with 2% bovine serum albumin (BSA) and incubated with anti-FLAG or anti-His primary antibody. The cells were incubated with anti-mouse IgG Alexa Fluor® 594-conjugated secondary antibody (Invitrogen) followed by staining with DAPI as described earlier. A Leica TCS Sp5 confocal microscope under a 63X oil immersion objective was used for imaging.

Live dead cell staining

CHP treated cells were washed with 1X PBS and stained using the Live/Dead BacLight Bacterial Viability Kit (Invitrogen). The cells were fixed with 4% PFA and imaged for SYTO9 dye (excitation at 480nm and emission at 500nm) and propidium iodide (excitation at 490nm and emission at 635nm) in a Leica TCS Sp5 confocal microscope.

Flow cytometry analysis

Various *Mtb* strains were grown to an exponential phase ($O.D._{600}$ of 0.3) in 7H9 medium followed by DAPI staining as described earlier. Approximately 10,000 cells were analysed by flow cytometry by exciting at 405 nm laser using 450/40 filter. The program BD FACS suite software was used to analyze the population distribution of *Mtb*, *MtbΔwhiB4 and whiB4-OE* strains and each population was represented by a unique color.

M-PFC

The entire ORF of *Mtb whiB4* (Rv3681), *sigB* (Rv2710), *sigE* (Rv1221) and *sigH* (Rv3223) were PCR- amplified from *Mtb* H37Rv genomic DNA using gene-specific oligonucleotides. The amplicons were digested with HindIII and MunI for *whiB4*, *sigB* and *sigH*, whereas with HindIII and EcoRI for *sigE* and ligated into similarly digested pUAB 400 vector. This bait plasmid was transformed into *Msm*. The subsequent transformed strain was then electroporated with *whiB4* cloned into pUAB300. Interacting clones were selected by plating transformants on 7H11 media containing KAN, HYG first and then screened by plating on 7H11 media containing KAN, HYG and TRIM (50 µg/ml). For the redox dependent assay, 0.5mM Diamide and 5mM DTT were added along with KAN, HYG and TRIM in the 7H11 media.

Macrophage and mouse infections

IFN-ɣ+LPS activated RAW 264.7 macrophages were infected with wt *Mtb*, *MtbΔwhiB4 and whiB4-OE* strains at a moi of 2 for 4 h, followed by treatment with amikacin to remove extracellular bacteria. After infection, cells were washed thoroughly with warm DMEM medium and resuspended in the same containing 10%

FBS. Samples were collected at the indicated time points, lysed using 0.06% SDS-7H9 medium and plated on OADC-7H11 agar medium for CFU determination.

BALB/c mice were infected via aerosol (Wisconsin-Madison) with the wt *Mtb* and *whiB4-OE* strain. To ensure the over-expression of WhiB4, doxycycline dissolved in water was supplied at regular intervals (every alternate day). The concentration of doxycycline was maintained at 1 mg/ml in 5% sucrose solution. At selected time point, three mice were killed and their lungs were removed and processed for analysis of bacillary load. Number of CFUs was determined by plating appropriate serial dilutions on 7H11 plates. Colonies were counted 3-4 weeks of incubation at 37°C.

Histopathology analysis was performed as described previously [9]. Briefly, sections of lungs were fixed in 10% neutral buffered formalin for embedding in paraffin, sectioning and staining with haematoxylin and eosin. A blinded examination of these sections from each mouse was carried out to evaluate the number of granulomas.

References

1. Ghosh S, Baloni P, Mukherjee S, Anand P, Chandra N. A multi-level multi-scale approach to study essential genes in *Mycobacterium tuberculosis*. BMC Syst Biol. 2013;7:132. doi: 10.1186/1752-0509-7-132. PubMed PMID: 24308365; PubMed Central PMCID: PMCPMC4234997.

2. Balazsi G, Heath AP, Shi L, Gennaro ML. The temporal response of the *Mycobacterium tuberculosis* gene regulatory network during growth arrest. Mol Syst Biol. 2008;4:225. doi: 10.1038/msb.2008.63. PubMed PMID: 18985025; PubMed Central PMCID: PMCPMC2600667.

3. Szklarczyk D, Franceschini A, Wyder S, Forslund K, Heller D, Huerta-Cepas J, et al. STRING v10: protein-protein interaction networks, integrated over the tree of life. Nucleic Acids Res. 2015;43(Database issue):D447-52. doi: 10.1093/nar/gku1003. PubMed PMID: 25352553; PubMed Central PMCID: PMCPMC4383874.

4. Cui T, Zhang L, Wang X, He ZG. Uncovering new signaling proteins and potential drug targets through the interactome analysis of *Mycobacterium tuberculosis*. BMC Genomics. 2009;10:118. doi: 10.1186/1471-2164-10-118. PubMed PMID: 19298676; PubMed Central PMCID: PMCPMC2671525.

5. Zeng J, Cui T, He ZG. A genome-wide regulator-DNA interaction network in the human pathogen *Mycobacterium tuberculosis* H37Rv. J Proteome Res. 2012;11(9):4682-92. doi: 10.1021/pr3006233. PubMed PMID: 22808930.

6. Wang Y, Cui T, Zhang C, Yang M, Huang Y, Li W, et al. Global protein-protein interaction network in the human pathogen *Mycobacterium tuberculosis* H37Rv. J

Proteome Res. 2010;9(12):6665-77. doi: 10.1021/pr100808n. PubMed PMID: 20973567.

7. Turkarslan S, Peterson EJ, Rustad TR, Minch KJ, Reiss DJ, Morrison R, et al. A comprehensive map of genome-wide gene regulation in *Mycobacterium tuberculosis*. Sci Data. 2015;2:150010. doi: 10.1038/sdata.2015.10. PubMed PMID: 25977815; PubMed Central PMCID: PMCPMC4413241.

8. Shannon P, Markiel A, Ozier O, Baliga NS, Wang JT, Ramage D, et al. Cytoscape: a software environment for integrated models of biomolecular interaction networks. Genome Res. 2003;13(11):2498-504. doi: 10.1101/gr.1239303. PubMed PMID: 14597658; PubMed Central PMCID: PMCPMC403769.

9. Chawla M, Parikh P, Saxena A, Munshi M, Mehta M, Mai D, et al. *Mycobacterium tuberculosis* WhiB4 regulates oxidative stress response to modulate survival and dissemination in vivo. Mol Microbiol. 2012;85(6):1148-65. Epub 2012/07/12. doi: 10.1111/j.1365-2958.2012.08165.x. PubMed PMID: 22780904; PubMed Central PMCID: PMC3438311.

10. Bhaskar A, Chawla M, Mehta M, Parikh P, Chandra P, Bhave D, et al. Reengineering redox sensitive GFP to measure mycothiol redox potential of *Mycobacterium tuberculosis* during infection. PLoS Pathog. 2014;10(1):e1003902. Epub 2014/02/06. doi: 10.1371/journal.ppat.1003902. PubMed PMID: 24497832; PubMed Central PMCID: PMC3907381.